

1 **Precipitation variability within an urban monitoring network**
2 **via microcanonical cascade generators**

3

4 Paweł Licznar^{1,*}, Carlo De Michele², Witłod Adamowski³

5 ¹ Institute of Environment Protection Engineering, Wrocław University of Technology,
6 Wrocław, Poland.

7 ² Department of Civil and Environmental Engineering, Politecnico di Milano, Italy.

8 ³ Institute of Environmental Engineering, John Paul II Catholic University of Lublin, Stalowa
9 Wola, 37-450 Poland.

10 *Corresponding author; email: pawel.licznar@pwr.edu.pl

11

12

13 **Abstract**

14 Understanding the variability of precipitation at small scales is fundamental in urban
15 hydrology. Here we consider as case study Warsaw, Poland, characterized by a precipitation-
16 monitoring network of 25 gauges, and as instrument of investigation the microcanonical
17 cascades.

18 We address the following issues partially investigated in literature: 1) the calibration
19 of microcanonical cascade generators in conditions of short time series (say, 2.5-5 yrs.); 2) the
20 identification of the probability distribution of breakdown coefficients through ranking
21 criteria; 3) the variability among the gauges of the monitoring network of the empirical
22 distribution of breakdown coefficients.

23 In particular, 1) we introduce an overlapping moving window algorithm to determine
24 the histogram of breakdown coefficients, and compare it with the classic non-overlapping
25 moving window algorithm; 2) we compare the 2N-B distribution, which is a mixed
26 distribution composed by two Normal (N) and one Beta (B), with the classic Beta distribution
27 to represent the breakdown coefficients using the Akaike information criterion; 3) we use the
28 cluster analysis to identify patterns of breakdown coefficient histograms among gauges and
29 timescales.

30 The scarce representation of the breakdown coefficients at large timescales, due to the
31 short period of observation (~2.5 yrs.), is solved through the overlapping moving window
32 algorithm. BDC histograms are described by a 2N-B distribution. A clear evolution of this
33 distribution is observed, in all gauges, from 2N-B at small timescales, to N-B at intermediate
34 timescales, and to Beta distribution for large timescales.

35 The performance of the microcanonical cascades is evaluated for the considered
36 gauges. Synthetic time series are analyzed with respect to the intermittency and the variability

37 of intensity, and compared to observed series. BDC histograms, for each timescale, are
38 compared among the 25 gauges in Warsaw, and with other gauges located in Poland and
39 Germany.

40

41 Key words: urban hydrology, precipitation time series, intermittency, microcanonical
42 cascade, overlapping window, randomization, cluster analysis.

43 **1 Introduction**

44 Urban hydrology requires the access to very precise information about the
45 precipitation variability over small spatial and temporal scales. Widespread use of surface
46 runoff models coupled to urban drainage networks increases the common request for rainfall
47 data inputs at high temporal and spatial resolutions. As it was already estimated a decade ago
48 by Berne et al. (2004), the necessary resolution of rainfall data, as input of hydrological
49 models, in Mediterranean regions, was about 5 min in time, and 3 km in space for urban
50 catchments of ~1000 ha. For smaller urban catchments of ~100 ha, even higher resolutions of
51 3 min and 2 km were required. Results obtained with the application of operational semi-
52 distributed urban hydrology models fully confirmed earlier observations on selected study
53 cases from England and France (Gires et al. 2012, 2013). These authors strongly recommend
54 the use of radar data in urban hydrology especially in context of real time control of urban
55 drainage systems. In particular, they opted for X-band radars (whose resolution is
56 hectometric), respect to the more common C-band radars, as affected by less uncertainty.
57 Additionally, Gires et al. (2012) stated that small scale rainfall variability, under 1 km
58 resolution, cannot be neglected, and should be accounted in probabilistic way in the real time
59 management of urban drainage systems. As a matter of fact, the implementation of radar

60 techniques gained a rising popularity in major cities across the EU (for details refer to
61 Appendix B, Thames Tunnel Needs Report, 2010).

62 Despite the obvious benefits of radar instruments, radar data are not always available
63 for practical applications. Thus, current versions of even most advanced computer rainfall-
64 runoff urban drainage models do not consider radar data as rainfall input. Therefore the only
65 possibility of accounting spatial rainfall variability is to consider different point time series for
66 each sub-catchment (Gires et al. 2012). The vast majority of engineering practical calculations
67 and modeling of drainage systems is still associated with point rainfall time series, or their
68 elaborations like intensity-duration-frequency (IDF) curves, or depth-duration-frequency
69 (DDF) relations, or simplified design hyetographs. This explains the necessity of high
70 temporal resolution of point rainfall measurements in urban catchments. It also has to be
71 noticed that time series at high temporal resolution (1-10 minutes) and with a considerable
72 record length (at least 20-30 years) are nowadays required especially from European
73 perspective with respect to the probabilistic assessment of the urban drainage network
74 functioning (Schmitt, 2000; European standard EN 752), or the probabilistic assessment of
75 retention volumes at hydraulic overloaded stormwater systems (Arbeitsblatt DWA-A 117).

76 The strategy of using local precipitation time series as basis of the probabilistic
77 assessment of urban drainage systems has two important shortcomings. In case of local
78 precipitation data shortage, this strategy fails completely. Whereas, in all other situations,
79 when some local precipitation datasets are accessible, questions and doubts about the
80 representativeness and reliability of data arise. First of all, the doubts regard the temporal
81 representativeness of data: short datasets could not allow to describe (as showed by Willems
82 2013) the multi-decadal oscillatory behavior of rainfall extremes in stormwater outflow
83 modeling. Other doubts regard the spatial representativeness of data: rainfall time series are
84 recorded only in a limited number of gauges installed in selected sub-catchments. This results

85 in assigning the same time series to a group of neighboring sub-catchments, or in critical but
86 not rare cases, one time series for the whole urban drainage system, habitually collected by a
87 gauge installed nearby the airport. Sometimes, in situation of local precipitation shortage, time
88 series from other locations are allowed by technical guidelines (Schmitt, 2000) only if there is
89 compatibility in terms of annual precipitation totals, and IDF values.

90 Finally, since most of the modeling activity is oriented to predict the future behavior
91 (e.g. in the next 50 yrs.) of drainage systems, the mere use of historical precipitation time
92 series of the last 20-30 years could not be significant to represent the future scenarios.
93 Alternatively, the generation of synthetic time series, from precipitation models, could
94 represent probable precipitation scenarios to feed hydrodynamic urban drainage models and
95 take into account the uncertainty associated to the discharge. However it should be pointed
96 out, that the information content of historical precipitation records is not increased by
97 precipitation models and synthetic data generation, which just provides an operational basis
98 for the extraction of such information.

99 Thus, there is a strong motivation for the development of local precipitation models at
100 high temporal resolutions. Many of them are based on the idea of precipitation disaggregation
101 in time. The disaggregation refers to a technique generating consistent rainfall time series at
102 some desired fine time scale (e.g. 5 min resolution) starting from the precipitation at a coarser
103 scale (e.g. daily resolution). At the same time, as it was stressed by Lombardo et al. (2012),
104 the downscaling techniques aim at producing fine-scale rain time series with statistics
105 consistent with those of observed data. A general overview of rainfall disaggregation methods
106 is given by Koutsoyiannis (2003). Among an ensemble of known techniques, random cascade
107 models, and especially microcanonical cascade models (MCMs) are quite often used. The
108 popularity of the latter ones could be explained by their appealing towards engineering
109 applications, the assumption of mass conservation (i.e. rainfall depth conservation) across

110 cascade levels, and straight rules for the extraction of cascade generators from local
111 precipitation time series (Cârsteanu and Foufoula-Georgiou 1996). Olsson (1998), Menabde
112 and Sivapalan (2000), Ahrens (2003), Paulson and Baxter (2007) provide contributions
113 demonstrating the potentiality of MCMs in rainfall downscaling. Molnar and Burlando (2005)
114 and Hingray and Ben Haha (2005) highlight the application of MCMs in urban hydrology.
115 Hingray and Ben Haha (2005) applied a continuous hydrological simulation obtaining from
116 synthetic rainfall series continuous discharge series used afterwards for the retention design.
117 Recently, Licznar (2013) illustrated the possibility of substituting synthetic time series
118 generated from MCMs to observed time series for the probabilistic design of stormwater
119 retention facilities.

120 Two decades of random cascade applications to precipitation disaggregation brought
121 progresses in the construction of generators. Quite soon, the assumption of independence and
122 identical distribution of the cascade weight generators, at all timescales, was questioned and
123 found suitable only for limited, rather narrow, range of analyzed scales (Olsson 1998, Harris
124 et al. 1998). As an alternative, Marshak et al. (1994), Menabde et al. (1997) and Harris et al.
125 (1998) promoted the use of the so-called “bounded” random cascade, for which its weights
126 distribution systematically evolves decreasing the weights variance with the reduction of
127 timescale. In addition, Rupp et al. (2009) suggested, that microcanonical cascade weights
128 should not be timescale-dependent only, but also intensity-dependent. The common practice
129 of assuming the Beta distribution for MCM generators was questioned by Licznar (2011a,b),
130 especially for sub-hourly timescales. Alternatively MCM generators were assumed Normal-
131 Beta (N-B) distributed with atom at 0.5, or 3N-B distributed, composed by three Normal and
132 one Beta distribution. For sake of clarity, it should be stressed that Beta refers sole to the
133 distribution of MCM generators, and has nothing in common with the beta β model, being the

134 simplest cascade model, often known as monofractal model (for details refer to Over and
135 Gupta 1996).

136 Molnar and Burlando (2008) explored the variability of MCM generators on a large
137 dataset of 10-min time resolution, including 62 stations across Switzerland. These authors
138 investigated seasonal and spatial variability in breakdown distributions to give indications
139 concerning the parameters' estimation of MCM in ungauged locations. To our knowledge,
140 there are only studies considering the large-scale variability (i.e. among different urban areas)
141 of MCM generators, and there is a lack of knowledge concerning the small-scale variability
142 (i.e. within an urban area).

143 It should be stressed that the fitting of cascade generators was relatively simple, but
144 extremely data demanding. Observational precipitation time series of high resolution
145 exceeding usually 20 years were unavoidable for cascade parameters fitting. This resulted in
146 the prevailing practice of comparing the statistics of synthetic and observed time series. In the
147 majority of studies, data originated from old type manual gauges were subject to obvious
148 uncertainty related to the precision of measurements, as well as the resolution of records
149 digitization. Simultaneously, the fitting of theoretical distributions to BDCs, in almost all
150 cases, was not supported by statistical tests confirming the correctness of achieved results, or
151 by the use of some information criteria to rank the theoretical distributions.

152 Having in mind the above discussed needs of urban hydrology, the current state of
153 MCMs, and being fully aware of the severe limitations of this rainfall disaggregation
154 technique, the goals of our study were:

- 155 1) Propose a methodology to calibrate microcanonical cascade generators in conditions
156 of short time series;
- 157 2) Identify the probability distribution of BDCs through the use of information criterion;
- 158 3) Investigate the variability of empirical BDCs distributions among a group of gauges;

159 4) Address the following questions of interest in urban hydrology: “Is it sufficient to use
160 a single time series for the probabilistic assessment of the entire urban drainage system? Is it
161 sufficient to fit just one MCM for the analysis of the whole city area? Could we continue the
162 practice of supplying urban rainfall-runoff models by time series recorded outside city center
163 by gauges located at the airport or over rural areas?”

164 **2 Data and Methodology**

165 **2.1 Data**

166 We use data belonging to a precipitation network of 25 gauges distributed throughout
167 517.24 km² of Warsaw city in Poland (Fig. 1). The dataset is the same used by Rupp et al.
168 (2012) and consists in a 1-minute precipitation (both liquid and solid) time series recorded by
169 electronic weighing-type gauges. All stations, TRwS 200E of MPS system Ltd. (Fig.2), were
170 installed and operated by the Municipal Water Supply and Sewerage Company (MWSSC) in
171 Warsaw. Prior to the network installation, studies about the location of the stations have been
172 done by the MWSSC to identify the best configuration, representative of the precipitation
173 variability within the urban area (Oke, 2006). Finding good places for installation of gauges
174 was possible due to the fact that the MWSSC in Warsaw operates a vast number of local
175 water intakes, water and sewage pumping stations. All these installations due to sanitary
176 standards have to occupy some terrain with green arrears around serving as buffers e.g. for
177 odors spread. In addition, all facilities are fenced and guarded for safety reasons. Thereby all
178 instruments were placed on grass, and their neighborhood met at least requirements of class 2
179 or 3, as recommended by WMO-No. 8. In the majority of gauges (i.e., R1, R3, R5, R7, R8,
180 R10, R12, R17, R18 and R19) it was possible to install them on flat, horizontal surface,
181 surrounded by an open area, meeting even requirements for class 1 instruments. In addition,

182 gauge R15 was installed in perfect conditions on the ground at the Warsaw Fryderyk Chopin
183 Airport.

184 Since the installation of the precipitation network in Warsaw was mainly motivated by
185 the real time control of the drainage system, all gauges (Fig. 1) were connected to a single
186 data acquisition system. The accuracy of gauge measurements, as claimed by manufacturer is
187 0.1%, and the data resolution is 0.001 mm for depth and 1 minute for time. As it was already
188 mentioned by Rupp et al. (2012), field tests, conducted prior to the operational use of the
189 precipitation network, have shown good agreement between simulated and recorded totals,
190 and have revealed a dampening/broadening of the input signal, evident over the range of a
191 few minutes. The last phenomenon - known as “step response error”- was studied in detail in
192 laboratory conditions for different gauge types by Lanza et al. (2005). These found that the
193 step error of TRwS gauge is quite small in comparison to other gauges, and equal to 3 minutes
194 in laboratory conditions. Our short 15-min field test (as displayed on Fig. 2) suggested a
195 dampening of gauge-recorded signal for the first 3-min initial phase of generated hyetograph
196 and its slightly longer 5-min broadening at the final phase of hyetograph. Detailed discussion
197 of the origins of gauge “step response” errors is beyond the scope of this manuscript, and in
198 fact is hard to be realized, since it is introduced by gauge inner microprocessor algorithm of
199 data processing. This algorithm is know-how of the gauge manufacturer, and is not reported
200 in the technical documentation. In general, it could be only stated that in weighing type
201 electronic gauges, the weight of deposited precipitation is sampled by some electronic (often
202 piezometric) sensor with some high temporal resolution at presumably kHz rate. Afterwards
203 all samples are averaged over longer time windows, unknown to the user. This process is
204 repeated for overlapping time windows, and the difference of the rainfall total of adjacent
205 windows is calculated to obtain the temporal rainfall rate reported as instrument output at its
206 recording time resolution. In addition, rainfall rates are always rounded regardless of the

207 magnitude of real precipitation (resulting in additional rounding errors discussed afterwards).
208 This procedure allows for satisfying smoothing of electronic sensor signal fluctuation due to
209 wind effects and temperature changes. It allows for the introduction of some additional filters
210 cutting sudden signal jumps due to foreign objects deposition inside open orifice of the gauge
211 inner tank (e.g. falling leaves or acts of vandalism by throwing small stones or garbage).

212 As a matter of fact in view of our personal experiences, and test results of WMO
213 (Lanza et al. 2005), it could be stated that reliable precipitation recording at single minute
214 scale by commercially available gauges is still the goal to be achieved, and not a current
215 reality. Having this in mind, as well as timescales of previous microcanonical cascade studies
216 concerning urban hydrology, realized on time series recorded by old-type gauges, we decided
217 to work with the aggregated precipitation time series at 5-minute resolution. The technique
218 used to aggregate original 1-min data into 5-min time series is discussed afterwards; here we
219 only mention that this operation was opposite to the rainfall total differentiation for adjacent
220 time windows operated by the gauge microprocessor.

221 Despite the limited timespan of available data, covering the period from the 38th week
222 of year 2008 up to the 49th week of year 2010, we believe that the Warsaw precipitation
223 network might support good probing ground for the variability study in the microcanonical
224 cascade parameters over small-scale urban areas. In fact, the Warsaw precipitation-monitoring
225 network belongs to the biggest European urban gauge networks. Its size could be compared
226 only with similar networks of 25 gauges in Vienna (414.87 km²), or 24 gauges spread
227 throughout Marseille (240.62 km²) and Barcelona (100.4 km²) (see Appendix B, Thames
228 Tunnel Needs Report, 2010).

229 We compare the results of our study with those related to other Polish and German
230 gauges. We limit our comparison to results previously published by Licznar et al. (2011a,b)
231 for four gauges in Germany (gauges A, B, C and D - representing local climates of different

232 parts of western Germany) and for one gauge in Wroclaw, Poland, and unpublished yet results
 233 by Górski (2013) for rain-gauge in Kielce, Poland (Fig. 3). Our choice is motivated by the
 234 similarity of the used methodology, and the investigated range of timescales, as well as by the
 235 indispensable accessibility to precise recordings of the breakdown coefficient histograms.

236 Finally, to investigate the existence of possible statistical bias induced by the
 237 calculation of BDCs on short precipitation records, we use additional data recorded by an old-
 238 type pluviograph gauge installed previously at the current location of gauge R7 on the ground
 239 of Lindley's Filters station. This pluviograph gauge was operated only in summer months
 240 from the May 1st to October 31st. Data were in the form of 15-min rainfall time series read
 241 off the original paper strips with the resolution of 0.1 mm for depth covering a period of 25-
 242 year from 1983 to 2007.

243 **2.2 Microcanonical cascade models**

244 We use microcanonical cascade models (MCMs) as in Licznar et al. (2011a,b). We
 245 consider the disaggregation of precipitation totals from 1280-min (quasi daily) into 5-min
 246 times series, assuming the branching number b equal to 2, and constructing cascades
 247 assembled from only 9 levels ($n=8, \dots, 1, 0$) corresponding to timescales $\lambda=2^n$ from $\lambda=256$ to
 248 $\lambda=1$ (Fig. 4). Precipitation depth time series generated by such cascades are the products of
 249 the original precipitation total R_0 at timescale $\lambda=256$ multiplied by the sequence of weights at
 250 the descending cascade levels:

$$251 \quad R_{j,k} = R_0 \prod_{i=1}^k W_{f(i,j),i}, \quad (1)$$

252 where $j=1, 2, \dots, 2^k-1$, 2^k marks the position in the time series at the k^{th} cascade step. The
 253 sequence of randomly generated weights $W_{f(i,j),i}$ is steered at the following i^{th} cascade step by
 254 the function $f(i,j)$, which rounds up $j/2^{k-i}$ to the closest integer. The weights in the

255 microcanonical cascades are forced to sum to one, so their pairs are always equal to W and $1-W$
 256 W respectively, where W is a two-sided truncated random variable from 0 to 1. The
 257 microcanonical assumption conserves the mass (precipitation depth in our case) at each
 258 branch, and eliminates the risk of cascade degeneration. From engineering perspective, this
 259 means that the downscaling process could be seen as opposite to precipitation summation
 260 realized by Hellman gauges, recording daily totals only, and a pragmatic solution for the
 261 generation of synthetic precipitation time series at 5-minute resolution.

262 In our study we do not focus our attention on the disaggregation capabilities of
 263 microcanonical cascades, already discussed in numerous papers. We concentrate on the small-
 264 scale variability of their generators W among gauges constituting the urban precipitation
 265 network. The obvious attractive of MCMs arises from the possibility of extracting the
 266 distribution of W from data on the base of breakdown coefficients studies (Cârsteanu and
 267 Fofoula-Georgiou 1996). By definition, BDCs are generally calculated using non-
 268 overlapping adjacent pairs of precipitation time series:

$$269 \quad BDC_{j,\tau} = \frac{R_{j,\tau}}{R_{j,\tau} + R_{j+1,\tau}} \quad j=1,3,5,\dots,N_\tau-1; \quad (2)$$

270 where $R_{j,\tau}$ is the precipitation amount for the time interval of length τ at position j in the time
 271 series, and N_τ is the length of time series at timescale τ . The calculation of BDCs with respect
 272 to Eq.(2) for Warsaw gauges is conducted only for nonzero pairs of R_j and R_{j+1} . Calculations
 273 are executed at aggregated intervals of length $2^n \tau_{org}$, where τ_{org} is the original time step equal
 274 to 5 min and n is a cascade level, increasing from 0 to 8, with increasing cascade timescales λ
 275 from 1 to 256 (Fig. 4). Simultaneously, for all analyzed timescales, BDC couples equal to 0 /
 276 1, or 1 / 0 (when only one between R_j and R_{j+1} is zero) are separated from resulting datasets

277 and their occurrence probabilities, respectively $p_0(LEFT)$ and $p_0(RIGHT)$ are used to estimate
278 intermittency probability p_0 :

$$279 \quad \Pr(BDC_n(j) = 0 \text{ or } BDC_n(j+1) = 0) = p_0(LEFT) + p_0(RIGHT) = p_0. \quad (3)$$

280 The probability p_0 is used within a MCM generator to take into account the intermittency, so
281 characteristic of precipitation, forcing some portion of random weights W to be equal to 0.

282 The preliminary results have revealed an over-representation of BDC values equal to
283 $1/2$ or $1/3$, $2/5$, $1/4$ (and $2/3$, $3/5$, $3/4$ respectively), especially for small timescales, i.e. $\lambda=1$
284 and $\lambda=2$. Fig. 5 (left panel) shows an example of BDC histogram for timescale $\lambda=1$, with
285 evident artificial spikes. Similar phenomenon was already reported by Rupp et al. (2009), and
286 Licznar et al. (2011b), and explained as the result of instrument or recording precision of
287 precipitation gauges. The magnitude of observed rounding errors for Warsaw gauges is
288 however smaller than in case of German gauges (Licznar et al., 2011b), because the
289 precipitation depths were recorded with better resolution of 0.001 mm still however resulted
290 in irregularity of BDCs distribution, induced by sharp peaks at discrete BDC values, and
291 hindered the identification of the theoretical distribution. In order to correct the rounding
292 errors, a randomization procedure originally proposed by Licznar et al. (2011b) was applied.
293 This type of procedure, also known as jittering, is fundamental in the analysis of data
294 characterized by the presence of ties, De Michele et al. (2013). Thus, the original 1-min time
295 series were slightly modified by adding to the precipitation depths, exceeding zero, some
296 random corrections. Random correction values were sampled from the Uniform distribution in
297 the range $[-0.0005, 0.0005]$ mm, resulting in visible BDCs histogram smoothing (Fig. 5 right
298 panel). Note, that the Uniform distribution is used for the randomization of the rounding
299 errors, because, in absence of information, it is the most intuitive distribution requiring less
300 assumption, for more details please see Licznar et al. (2011b).

301 Irregularities in BDC histograms were observed for timescales $\lambda > 8$. These are due to
302 the decreasing sample size, calculated on limited timespan of accessible data, slightly
303 exceeding 2 years. This issue was rather irrelevant in former studies (Molnar and Burlando
304 2005, 2008, Licznar et al. 2011a,b) realized on data series 10 or even 20 times longer. To
305 solve this issue, we applied the overlapping moving window algorithm as an alternative to the
306 classical non-overlapping moving window algorithm for the calculation of BDCs values.
307 Figure 6 shows the differences between the two algorithms for $\lambda = 1$. Switching from non-
308 overlapping to overlapping moving window algorithm leads to increase the number of time
309 segments for the calculation of BDCs values. For time series of n data, and a time window of
310 size $m \leq n$, the number of non-overlapping windows is $\lfloor n/m \rfloor$, where the symbol $\lfloor \cdot \rfloor$ represents
311 the integer part, while the number of overlapping windows is: $(n-m+1)$. For large $n \gg m$, the
312 overlapping moving window algorithm leads to almost m times the number of time segments
313 available in the overlapping moving window algorithm. It should be underlined that the real
314 strength of the overlapping moving window algorithm in analyzing distributions of BDCs
315 values could be observed for the largest timescales. The reason is that for small timescales,
316 most of time segments is characterized by zero precipitation, and thus not involved in the
317 calculation of BDCs, whereas for larger timescales, time segments are becoming larger and
318 rarely characterized by zero precipitation. This phenomenon arises from the fractal properties
319 of rainfall time series, and similar conclusions result from the “box-counting” analysis.

320 It is clear that the overlapping moving window algorithm is especially desired for
321 limited observational datasets. However, its implementation for short time series may be
322 characterized by a poor representativeness of BDCs distributions, due to multi-decadal
323 oscillations of precipitation totals and extremes (Willems 2013). To investigate the magnitude
324 of the oscillations in the BDCs distributions, we use historical time series from former old-

325 type gauge R7, covering a 25-year period, from 1983 to 2007 at 15-min resolution. For each
326 year, there are available only 6 months of data from May to October. For this dataset, we
327 make the calculations of BDCs in 7 time periods. First, we calculate BDCs for the following
328 5-year periods: 1983-1987, 1988-1992, 1993-1997, 1998-2002 and 2003-2007 using the
329 overlapping moving window algorithm. We consider this temporal size (5 years \times 6 months =
330 30 months) because comparable to the one available for electronic gauges. Afterwards, we
331 repeat the same calculation with a 25-year long size using both non-overlapping and
332 overlapping moving window algorithms. As we work here with a coarser resolution (15-min
333 instead of 5-min of electronic gauges), we decide to perform the analysis with a smaller
334 hierarchy of sub-daily timescales λ' from 1 to 32 and breakdown times from 15-30 min up to
335 480-960 min. For all calculations we perform the randomization of nonzero values. Since
336 their reading precision was set to 0.1 mm, we introduce a random correction belonging to the
337 Uniform distribution in the range [-0.05, 0.05] mm.

338 To compare BDC histograms, obtained for all analyzed timescales λ and λ' , with
339 theoretical functions, a probability distribution assembling 2 truncated (with truncation points
340 at 0 and 1) Normal distributions (Robert, 1995), and 1 Beta symmetrical distribution was
341 implemented. This distribution, indicated as 2N-B distribution, has the following density
342 function:

$$343 \quad p(w) = p_1 \left\{ \frac{1}{\sigma_1 \sqrt{2\pi}} e^{-\frac{(w-0.5)^2}{2\sigma_1^2}} \right\} + (1-p_1) \left\{ \frac{1}{B(a)} w^{a-1} (1-w)^{a-1} \right\} + (1-p_2) \left\{ \frac{1}{\sigma_2 \sqrt{2\pi}} e^{-\frac{(w-0.5)^2}{2\sigma_2^2}} \right\} \quad (4)$$

344 where p_1 and p_2 were weights characterizing the contribution of the individual distributions
345 within the 2N-B distribution, σ_1 and σ_2 were the scale parameters of truncated Normal
346 distributions, and $B(a)$ was the symmetrical Beta function, parameterized by a .

347 The fitting of 2N-B distribution parameters was performed numerically by means of
348 maximum likelihood estimation. It is very likely, that the use of the model given in Eq.(4),
349 governed by 5 parameters, could suffer of an over-parameterization, in comparison to the
350 most commonly used Beta symmetrical distribution with only 1 parameter. Note that the
351 application of goodness-of-fit tests (namely Kolmogorov-Smirnov test or χ^2 test) at 1% or 5%
352 levels of significance gave negative result as for Beta as for 2N-B distribution. This because
353 the large sample size of empirical BDCs has led to the rejection of the hypothesis, even in the
354 case of very small differences between observed and theoretical distributions, as pointed out
355 also in Licznar et al. (2011a). Here, we use the Akaike information criterion *AIC*, as a
356 measure of the relative quality between 2N-B and Beta models for given sets of empirical
357 BDCs. *AIC* is the maximized value of the log-likelihood function (*LL*) penalized by the
358 number of model parameters *k*:

$$359 \qquad \qquad \qquad AIC=2k-2LL \qquad \qquad \qquad (5)$$

360 The preferred distribution is the one with the minimum value of *AIC*.

361

362 **2.3 Cluster analysis**

363 To our knowledge, until now, the variability of MCM generators among a group of
364 gauges was investigated comparing the value of the parameter of Beta distribution (Molnar
365 and Burlando 2008). Here, we preferred to compare directly the empirical distribution of
366 BDCs instead of the parameters of the theoretical distribution, possibly biased by fitting
367 errors. We have encountered the same problems found in the implementation of statistical
368 tests due to the large sample size. For this, we have used the cluster analysis to compare the
369 shape of BDC histograms among the stations of the monitoring network in Warsaw, and with
370 other Polish and German gauges.

371 In particular a *hierarchical clustering* is used. This is a data-mining tool, applied to
372 segment data into relatively homogeneous subgroups, or clusters, where the similarity of the
373 records within the cluster is maximized (Larose, 2005). Prior the application of the cluster
374 analysis, for each timescale and each site, the BDC histogram is sampled in 100 points,
375 selected at equal distance one from the following one. These 100 values are the components
376 of a vector representing the empirical BDC distribution. Note that a basic requirement of
377 cluster analysis is the comparison of records of equal length. As, all BDCs distributions are
378 left and right truncated, in the interval (0,1), sampling their histograms with a resolution of
379 0.01 produces vectors, which describe well the shape of histograms. The clustering of these
380 vectors (searching similar sites) is operated using the Euclidean distance. It is computed as:

$$381 \quad d_{Euclidean}(X, Y) = \sqrt{\sum_i (x_i - y_i)^2}, \quad (6)$$

382 where x_i and y_i with $i=1, \dots, 100$, represent respectively the i -th component of X and Y vectors.

383 The Euclidean distance is a measure of similarity, not having, in general, a physical
384 interpretation. Initially, in hierarchical clustering analysis, each vector is considered to be a
385 tiny cluster of its own. Then, in following steps, the two closest clusters are aggregated into a
386 new combined cluster. By replication of this operation, the number of clusters is reduced by
387 one at each step and eventually, sites are combined into a single huge cluster. During the
388 agglomerative process, the distance between clusters is determined based on single-linkage
389 criterion. In this case, the distance between two clusters A and B is defined as the minimum
390 distance between any element in cluster A and any element in cluster B. With respect to this
391 single-linkage is often termed the nearest-neighbor approach, and tends to form long, slender
392 clusters, clearly indicating similarities among clustered elements. As a final result of
393 agglomerative clustering a treelike cluster structure (named dendrogram) is created.

394 Dendrograms show similarities, as well as dissimilarities, of BDC distributions among
395 the considered sites and they are prepared separately for all analyzed timescales. In addition,
396 the cluster analysis is also applied to the intermittency parameter, comparing in this case,
397 vectors of 8 components, each of these being the p_0 value for the 8 timescales
398 $\lambda=1,2,4,8,16,32,64,128$.

399

400

401 **3 Results and Discussion**

402 Results are presented relatively to gauge R7, for brevity. This station has been selected
403 because of its localization in the strict city center, its installation in perfect meteorological
404 conditions on the ground, and the existence of former historical rainfall records. Results for
405 the other gauges are qualitatively similar to those shown for R7.

406

407 **3.1. Empirical BDCs distributions**

408 BDCs histograms are calculated using the non-overlapping moving window algorithm,
409 and plotted in Fig. 7 for gauge R7 and a sequence of analyzed breakdown times. It is clearly
410 visible that despite the randomization procedure removes pronounced peaks of histograms at
411 certain specific BDC values, like 0.5 or 1/3, 2/5, 1/4 and 2/3, 3/5, 3/4 respectively (Fig. 5), the
412 plots especially for timescales exceeding $\lambda=8$ remain still irregular, reducing the possibility of
413 identifying the proper theoretical distribution. Visible irregularities of BDC histograms
414 increase with increasing timescales, which is an obvious effect of decreasing datasets and thus
415 decreasing populations of calculated BDC values not allowing to produce histograms of fine
416 bins resolution. Similarly, Fig. 8 reports the distributions of BDC calculated through the

417 overlapping moving window algorithm. The comparison between Fig.7 and Fig.8 shows how
418 the change of algorithm from non-overlapping to overlapping moving window has brought to
419 evident smoothing of BDC histograms especially for larger timescales, but occurring also at
420 small timescales. Note that the smoothness of BDC histograms in Fig. 8 is comparable with
421 the quality of BDC histograms showed by Licznar et al. (2011b) for German gauges, derived
422 using non-overlapping moving window algorithm for much longer precipitation time series
423 ranging from 27 to 46 years of continuous records. The introduction of the overlapping
424 moving window algorithm allowed for the fitting of MCM parameters in the case of Warsaw
425 gauges with the availability of extremely short time series (say 2 years long). The overall
426 acceptance of overlapping moving window algorithm implementation, also for short rainfall
427 time series is discussed in paragraph 3.3.

428

429 **3.2. Theoretical BDCs distributions and their evolution along timescales**

430 In Fig. 8, we report also the fitted theoretical distributions (2N-B distribution in solid
431 red curves, and Beta distribution in blue dashed lines) for each timescale considered. The
432 visual comparison clearly indicates a better fit of 2N-B (or N-B in some cases) distribution for
433 timescales smaller than $\lambda=64$. In Fig.8, it is possible to see how the distribution with the best
434 fit changes from a Beta distribution (B) at $\lambda=128$, to a joined double Normal-Beta distribution
435 (2N-B) for the smallest value of λ , through a joined Normal-Beta distributions (N-B). This is
436 in agreement with previous studies by Licznar et al. (2011a,b). This observation is supported
437 by higher values of log-likelihood for 2N-B distribution (or the simplified N-B) in comparison
438 to the Beta distribution (Tab. 1). These differences are in the range of thousands, and even
439 after accounting for the number of model parameters, the AIC for 2N-B (or the simplified N-
440 B) distributions are much smaller (or equal) the one of Beta distributions, confirming the

441 visual result given in Fig. 8. Based on this, we prefer the 2N-B distribution respect to the Beta
442 distribution, except for the case $\lambda=128$. Analyzing the data reported in Tab. 1, it is worth to
443 notice the systematic increase of sample size n increasing the timescale.

444 From the practical point of view a rapid increase in the number of BDCs, equal or
445 close to 0.5, decreasing the timescale should be expected, as a symptom of enclosing a limit
446 of the precipitation temporal variability in a point by accessible instruments. The precipitation
447 averaging over some small area of orifice and time intervals is inevitable for gauges, thus for
448 small timescales most of small scale precipitation variability remains undetected and
449 smoothed leading to an over-representation of constant precipitation time intervals. From the
450 theoretical point of view, it should be noticed that bounded cascades allow the multiplicative
451 weights (or precisely their distributions) to depend on the cascade level and converge to unity
452 as the cascade proceeds. As a consequence, the simulated random process becomes smoother
453 on smaller timescales (Lombardo et al. 2012), which in general mimics the dynamics of
454 precipitation collected by gauges. In other words as it was postulated by Marshak et al.
455 (1994), Menabde et al. (1997) and Harris et al. (1998), the variance of weights reduces with
456 every descending cascade level. As a simple extension of this rule, the increasing frequency
457 of weights at the central part of their distribution plots has to be observed. The increase in the
458 number of BDCs equal or close to 0.5 with decreasing timescale is well illustrated by
459 empirical histograms at well-known pioneering contributions to MCM applications for
460 rainfall time series disaggregation, published by Olsson (1998), Menabde and Sivapalan
461 (2000) and Guntner et al. (2001). Quite recently, this behavior was also proved to be rainfall
462 intensity dependent by Rupp et al. (2009).

463 For each analyzed timescale, we have estimated the parameters of 2N-B probability
464 distribution (or its simplifications N-B and B): p_1 , p_2 , a , σ_1 and σ_2 . Table 2 gives the values
465 for gauge R7 with their 95% confidence limits. A good visual fit of empirical BDC

466 distributions in Fig. 8 corresponds to quite narrow 95% confidence limits of the fitted
467 parameters (mostly invisible on Fig. 9 plots). The 95% confidence limits are not exceeding
468 few percent of the estimated values, with the sole exception of parameter p_1 for $\lambda=4$, where
469 the differences range up to 27%. Additionally, the scale parameters of Normal distributions,
470 σ_1 and σ_2 , appear to be constant among analyzed timescales, not only for gauge R7, but also
471 for the other Warsaw gauges.

472 The variability of p_1 , p_2 , a with λ is presented in Fig. 9 for gauge R7. A systematical
473 decrease of p_1 down to 0 increasing the timescale is observed, denoting a decreasing
474 importance of the first Normal within the 2N-B distribution. An opposite systematical
475 increase of p_2 up to 1 increasing the timescale is observed, denoting a decreasing importance
476 of the second Normal within the 2N-B distribution. The evolution of the Beta parameter a
477 shows a fast reduction with below 1 values noticed for the smallest scales, yielding the change
478 of Beta distribution shape from convex to concave. At larger timescales, the reduction of a is
479 hardly visible with the sole exception of $\lambda=128$. Figure 10 shows the variability of
480 intermittency parameters p_0 with timescale λ . For all of them, the values of $p_0(LEFT)$ match
481 the values of $p_0(RIGHT)$, which is in good agreement of previous studies of Molnar and
482 Burlando (2005) and Licznar et al. (2011a, 2011b). This could be interpreted as the proof of
483 fully random occurrence of intermittency in the precipitation time series. Systematical
484 increase of p_0 with λ is observed with the sole exception of some small drop at $\lambda=128$.
485 General increase of p_0 with timescale is a natural outcome of fractal properties of the
486 geometric support of rainfall occurrence.

487

488 **3.3. Performance of the overlapping moving window algorithm**

489 The performance of the overlapping moving window algorithm was investigated in
490 detail at gauge R7, where a 25-year long time series at 15-min resolution was available. We
491 calculate the parameters of 2N-B distribution for the hierarchy of sub-daily timescales λ'
492 relatively to the following 5-year periods: 1983-1987, 1988-1992, 1993-1997, 1998-2002 and
493 2003-2007 (indicated in the next with the roman numbers I,II,...,V respectively) and the whole
494 25-year dataset (indicated in the next with case A) using the overlapping moving window
495 algorithm. In addition, we calculate the parameters of 2N-B distribution also using the
496 classical non-overlapping moving window algorithm over the whole 25-year dataset
497 (indicated in the next as case B). The results are shown in Figs. 11-13.

498 In general, the selected probability distribution was a Beta for the largest timescales
499 ($\lambda'=16, 32$), a N-B for $\lambda'=2,4,8$, and a 2N-B distribution for $\lambda'=1$ (with the only exception of
500 the period IV). The above listed timescales λ' are not compatible with timescales λ , however
501 transposing them on a coherent time axis leads to the conclusion that characteristic transitions
502 from Beta to N-B and 2N-B distributions occurred at approximately the same time ranges.
503 The estimated parameters σ_1 and σ_2 appeared to be constant among analyzed timescales, and
504 equal to 0.0646 and 0.1363 respectively. These values were very close to those reported in
505 Tab. 2. Fig. 11 shows the estimates of p_1 , for $\lambda'=1$, with a variability in the range 0 -- 0.058
506 for the 5-year periods I-V. At the same time, the 95% confidence limits of p_1 overlap partially
507 one on the other, and with values estimated for cases A and B. Confidence limits for periods
508 I-V are rather wide and are reduced of 50% only for cases A and B. Note that here we work
509 with 15-min time series, and not 1-min time series as before.

510 A better agreement was observed for larger timescales, as illustrated in Figs. 12 and
511 13, with visibly narrow 95% confidence limits, but still partial overlapped one on the other.
512 For smaller timescales, larger oscillations of p_2 parameter could be observed over the periods

513 I-V, but due to wider 95% confidence limits, they overlap one on the other and with those
514 relative to cases A and B. The only exception is found for the period III at timescale $\lambda'=1$.

515 For parameter a and $\lambda'=1$, 95% confidence limits for all calculations overlap with the
516 only exception of period V, having slightly lower values. For $\lambda'=2$ and $\lambda'=4$, mutual overlay
517 of 95% confidence limits was noticed. Passing to $\lambda'=8$ and $\lambda'=16$, the overlapping among all
518 pairs of periods from I to V was not always present, but present with 95% confidence limits
519 drawn for case B. For $\lambda'=32$, 95% confidence limits for periods I-V and case A were
520 extremely narrow.

521 Results reported above suggest good repeatability of BDCs distributions calculated
522 during all periods, which finds its graphical confirmation in Fig. 14, with the only exception
523 of period II and timescale $\lambda'=1$. Probably this could be explained by the poor performance of
524 newly proposed overlapping moving window algorithm applied to low time resolution of the
525 original time series. Our observations support the use of overlapping moving window
526 algorithm for BDCs calculations in situations of short (about 2-year) precipitation time series
527 access, while in previous microcanonical cascade studies (e.g. Molnar and Burlando 2005 and
528 2008) longer (e.g. about 20-30 years) time series were indispensable. In addition, even in
529 situations of longer precipitation time series access, BDCs calculations by means of proposed
530 algorithm should be favored relative to old non-overlapping moving window technique, as the
531 new algorithm leads to narrowed 95% confidence intervals of fitted BDCs distributions
532 parameters.

533 We do not claim here, that the moving window technique combined with MCMs
534 solves the problem of local precipitation time series shortage. It is obvious that rainfall
535 statistics derived from short periods may be biased against long-term statistics (e.g. due to
536 climate oscillations). Until now to our best knowledge, there were no attempts made to assess

537 the possible bias of MCMs generators due to precipitation oscillations, driven by climate
538 change. Hitherto contributions of MCMs generators were mostly based on relatively not too
539 long precipitation series, presumably displaying only very weak if any oscillations and were
540 always treated as single dataset.

541 Possible bias of MCMs generators due to precipitation oscillations undoubtedly should
542 be verified on other much longer time series of better resolution like for example the 10-min
543 time series collected at Uccle, Belgium (Willems 2013). Simultaneously, only detailed
544 analysis based on long and complete precipitation time series covering at least few decades
545 could deliver us the answer to this question, if the climate change effect could be retrieved via
546 the temporal evaluation of microcanonical cascade generators. From this perspective, the
547 moving window technique could be of considerable usefulness in BDCs distributions fitting
548 for periods corresponding to 11 yrs solar spot cycles.

549

550 **3.4. Performance of microcanonical cascade in disaggregation**

551 As additional check of the overall performance of the applied techniques (i.e., the
552 randomization procedure, the overlapping moving window algorithm and the 2N-B
553 probability distribution), we test the performance of microcanonical cascade in disaggregating
554 the precipitation at the analyzed gauges. The MCM is used to generate 100 synthetic time
555 series at 5-min resolution on the basis of the observed 1280-min precipitation totals (similarly
556 to Molnar and Burlando 2005, Licznar et al. 2011a and b). To evaluate the goodness of
557 disaggregation, we compare the probability of zero precipitation at synthetic and observed
558 time series for all analyzed timescales. Moreover, we calculate the survival probability
559 function of nonzero synthetic precipitation amounts and compare it to the survival probability
560 function observed precipitation amounts. This analysis is limited to 5-min data, i.e. terminal

561 results of the disaggregation, most suitable for urban hydrology application. Special interest
562 on the 5-min synthetic time series was also focused by other researchers (see e.g., Molnar and
563 Burlando 2005 and 2008, Licznar et al. 2011a and b). An example of 56.3 mm event
564 disaggregation is plotted in Fig.15, for gauge R7. It should be stressed that the structure of the
565 synthetic time series is composed by uncorrelated segments like the one presented in Fig.15.
566 Thus, the synthetic time series is missing the correct autocorrelation structure of natural
567 precipitation (for detail discussion see: Lombardo et al. 2012). The expected value of the zero
568 precipitation probability, $E(p_0)$, for observed and generated series is given in Fig. 16, for
569 gauge R7. The synthetic values of $E(p_0)$ are calculated as average over 100 MCM
570 disaggregations. The differences in terms of $E(p_0)$ between observed and simulated are
571 negligible (see Fig. 16). In addition, for comparison, we give also the synthetic values of $E(p_0)$
572 for gauges R15 and R25.

573 Fig. 17 shows the comparison between observed and simulated survival probability
574 function of rainfall amount at 5-min, for gauge R7. In Fig. 17, for gauge R7, we report the
575 empirical survival probability function for a synthetic series out of 100, and the averaged
576 function using all the generated series. In addition, for comparison, we give also the averaged
577 survival functions for gauges R15 and R25. At first glance, highest rainfall intensities drawn
578 in Fig. 17 show strange behavior manifested by constant exceedance probability above a
579 given precipitation threshold. This is especially pronounced for observed or synthetic series
580 from a single MCM run. This is due to the very short rainfall time series used for the
581 calculation of survival probability functions. According to multifractal theory, singularities in
582 small dataset are very rare. Highest rainfall intensities as singularities are very rare in 2-year
583 long series. The behavior of both the synthetic functions for gauge R7 in Fig. 17 is very
584 similar, with the sole exception of the extended and smoothed tail of the averaged function
585 plot. Both the synthetic functions are placed above the observed function. This displacement

586 reveals over-prediction of 5-min precipitation depths, particularly at the range of intensities
587 from 0.3 mm/5min to about 2.0 mm/5min. It should be noticed, that the magnitude of
588 dissimilarities between synthetic and observed survival functions for gauge R7 did not exceed
589 the ones reported in other works, see e.g., Molnar and Burlando (2005), Licznar et al.
590 (2011a,b). In comparison, the magnitude of dissimilarities between observed survival
591 probability for gauge R7 and synthetic (average) survival probability function for other
592 gauges R15 and R25 was much more pronounced.

593

594 **3.5. Cluster analysis results and their interpretation**

595 Dendrograms summarizing the results of the cluster analysis for BDC histograms are
596 produced for each timescale, and reported in Figs 18 and 19 only for $\lambda=1$ and $\lambda=128$,
597 respectively. Results for the first four timescales, i.e. $\lambda= 1,2,4,8$, are unsurprising and easy to
598 be interpreted. All Warsaw gauges are grouped in a single cluster with similar shapes of BDC
599 histograms. For all Warsaw gauges their interconnection on the dendrogram is placed at the
600 level of binding distance equal to about 0.5. Only R25 seems to be characterized by slightly
601 different pattern of BDC histogram. However, gauge R25 has a behavior, which is still much
602 closer to other Warsaw gauges, rather than the behavior of the other cities considered. For
603 example, at $\lambda=1$, gauge R25 is merged into Warsaw gauges cluster at an Euclidean distance
604 equal to 0.81, whereas the same occurs for Kielce (the closest considered Polish city) gauge at
605 the Euclidean distance equal to 1.07. For other timescales, $\lambda= 2, 4, 8$, gauge R25 merges the
606 cluster of Warsaw gauges at quite similar Euclidean distances: 0.89, 0.83 and 0.81
607 respectively.

608 The dendrogram for $\lambda=128$ is given in Fig. 19, being representative of timescales
609 $\lambda=16,32,64,128$. From Fig.19, it is possible to see the departure of gauge R15 from the cluster
610 of other Warsaw gauges. The position of gauge R15 is isolated from other Warsaw gauges
611 and its Euclidean distance from the closest one is large, and increases with greater timescale;
612 it is equal to 1.80, 3.19, 3.88, and 8.03 respectively for $\lambda=16, 32, 64$ and 128. Simultaneously,
613 the Euclidean distance from the cluster of Warsaw gauges to the nearest neighbor does not
614 exceed 0.90, 1.00, 1.40 and 1.89 respectively for $\lambda=16, 32, 64$ and 128.

615 This last observation puts in evidence that in general the variability of BDC shapes,
616 among Warsaw gauges, increases with greater timescale. It may partly be explained by the
617 already mentioned evolution of histogram shapes, and the replacement of 2N-B distribution
618 by less centered N-B and finally B distribution characterized by a higher variance of BDC. In
619 the specific case of gauge R15, its BDC histograms for the largest timescales are boldly
620 concave (not shown for brevity) and their shapes are becoming similar to Beta symmetrical
621 distributions parameterized by very small values of a : 0.76, 0.64, 0.54, and 0.45 respectively
622 for $\lambda= 16,32, 64$, and 128.

623 As last step, we used the cluster analysis to investigate the variability among the
624 gauges, in terms of the intermittency parameter p_0 considered as a vector having as the 8
625 components its values in correspondence of the considered timescales. Results are given in
626 form of dendrogram in Fig. 20. With respect to p_0 , all Warsaw gauges form one single chain-
627 like cluster. Three gauges in the cluster, namely R14, R25 and R15, are characterized by the
628 largest distances from the nearest neighbor with Euclidean distances equal to: 0.079, 0.064
629 and 0.0614 respectively. The distance of gauges R15 and R25 from the other stations in
630 cluster is similar to observations made for Figs. 18 and 19. A possible, but not certain,

631 explanation for gauge R14 could be its location close to gauge R15, in a weak-developed part
632 of the city.

633 Unfortunately, we do not have access to other meteorological data to compare our
634 results with other local climate conditions. To our knowledge, studies about microclimate or
635 local turbulence were not conducted for Warsaw. However in our opinion, the anomalous
636 behavior of gauges R15 and R25 does not originate from random errors due to gauges
637 installation. As it was mentioned before, all gauges were installed in very good conditions,
638 and R15 was an airport gauge. A plausible explanation of the anomalous behavior of gauges
639 R25 and R15 could be found in its location. Gauge R25 location is on south-east suburban
640 area, in the close vicinity of forested area and Vistula river valley. This specific suburban area
641 is also most frequently a place for the development of local convection processes (prof. S.
642 Malinowski, personal communication, 2013). The anomalous behavior of gauge R15 seems to
643 arise from its specific location on the ground of the Warsaw airport. In the neighborhood of
644 the instrument there are no high buildings and trees and the ground is covered only by short
645 cut grass. The local atmospheric turbulence conditions, additionally influenced by taking off
646 and landing aircrafts could have favored the different behavior of this station. In general,
647 gauges R15 and R25 are the only instruments, installed outside the areas of urban fabric (Fig.
648 1) in rather rural conditions of surrounding green areas. The suburban location of these gauges
649 connected with direct green surrounding reduces, or even minimalizes to zero, urban heat
650 island effects. Peng et al. (2011) investigated the surface urban heat island intensity across
651 419 global big cities (including Warsaw city). These authors showed that the distribution of
652 daytime surface urban heat island intensity correlates negatively across cities with the
653 difference of vegetation fractional cover, and of vegetation activity, between urban and
654 suburban areas. Kłysik and Fortuniak (1999) for the second big city of Poland, Łódź (about
655 120km south-west) comparable to Warsaw flat topography, found the occurrence of the urban

656 heat. According to statistics calculated over many years, in two stations one in center and one
657 in airport, over 80% of nights were characterized by a surplus heat in town, amounting 2-4°C,
658 and sporadically to 8°C and more. Once more for Łódź, Fortuniak et al. (2006) confronted the
659 data from two automatic stations: one urban and one rural. They found the relative humidity
660 to be lower in the town, sometimes by more than 40%, and water vapour pressure differences
661 to be possibly either positive (up to 5 hPa) or negative (up to -4 hPa). Air temperature
662 differences between the urban and rural station exceeded 8°C. It could be that similar
663 processes occur in Warsaw and affect local precipitation dynamics, and gauges R7 and R15
664 and R25. As consequence, statistics of synthetic time series vary visibly in Figs. 16 and 17.
665 However, the significance of these differences should be studied in more details in the future.

666 **4 Conclusions**

667 Owing in mind the simplicity of microcanonical cascade generators retrieval from
668 observational data, we proposed to use this technique for the local variability of very short
669 precipitation time series within an urban monitoring network.

670 We considered a network of 25 gauges deployed in Warsaw city (Poland) over an area
671 of 517.2 km². An attempt was made to define the generators of a MCM applicable for
672 producing 5-min time series, as requested by urban hydrologists, through the disaggregation
673 of quasi-daily precipitation totals. We showed that smooth distributions of BDC are possible,
674 for all analyzed timescales, even in case of limited length of time series, which in our case
675 slightly exceeded 2 years only. This was made possible by the implementation of a
676 randomization procedure and the use of an overlapping moving window algorithm for the
677 calculation of BDCs.

678 The correctness of the overlapping moving window algorithm is checked using
679 additional 15-minute rainfall time series, 25-year long, at gauge R7. The algorithm is

680 implemented for a hierarchy of sub-daily timescales, and separate 5-year periods. The results
681 of BDC calculations are compared to those obtained using all 25 years of data with both
682 overlapping and non-overlapping moving window algorithms. Despite the coarse resolution of
683 data, and winter time gaps in the series, the results show a good agreement of BDC
684 distributions calculated over the different periods, suggesting the correctness of the
685 overlapping moving window algorithm, at least in central Poland.

686 To adequately describe the shapes of BDC histograms, we have implemented a special
687 joined probability distribution, 2N-B, assembled from 2 Normal distributions and 1 Beta
688 symmetrical distribution. A systematical evolution of BDC histograms from joined double
689 Normal-Beta distributions (2N-B), through joined Normal-Beta distributions (N-B) up to Beta
690 distributions (B) was observed increasing the timescale. To test the use of more complicated
691 models alternative to the classical Beta distribution, we suggested the Akaike information
692 criterion (AIC).

693 To check all the applied techniques (i.e., the randomization procedure, the overlapping
694 moving window scheme and the 2N-B distribution), MCMs were used to disaggregate 1280-
695 min precipitation into 5-min time series. The quality of the generated series was checked
696 comparing the statistical properties of these with the ones of observed series. In particular, we
697 compared probabilities of zero precipitation and the survival probability functions of non-zero
698 5-min precipitation amounts, for the considered timescales, with agreement comparable to
699 previous studies made in Switzerland, Germany and Poland.

700 As main part of this study, we have conducted an intercomparison of BDC histograms
701 among the 25 Warsaw gauges, and considering as a term of reference also other 6 gauges
702 located in Poland and Germany. The intercomparison was made, scale-by-scale, by means of
703 cluster analysis. Resulting dendrograms for small timescales (i.e. $\lambda=1,2,4,8$) revealed rather
704 small variability of BDC histograms among all Warsaw gauges in comparison to the

705 variability exhibited with respect to the other external gauges. Only gauge R25 seems to be
706 characterized by a slightly different pattern. It might originate from the specific gauge
707 location on the city boundary, in the vicinity of forested areas and Vistula river valley.

708 Dendrograms obtained for large timescales (i.e. $\lambda=16, 32, 64, 128$) also delivered a
709 general picture of similarity among Warsaw gauges, with the very clear exception of gauge
710 R15. To our best knowledge a possible explanation of this was its installation on the ground
711 of the Warsaw airport, strongly man-modified and with local turbulence conditions. In
712 addition, R25, R15, and R14 were also identified as gauges presenting slightly different
713 behavior in terms of the intermittency parameter p_0 .

714 As final remarks, we can affirm that MCMs combined with cluster analysis could be
715 used as a tool for the assessment of the spatial variability of local precipitation patterns among
716 a group of gauges. This framework could be effectively implemented even in case of very
717 short observational series thanks to the proposed overlapping moving window algorithm. We
718 believe that the use of this algorithm could increase the development and use of MCMs in
719 urban hydrology. At the same time, we are fully aware of the inherent MCM limitations in the
720 quality of rainfall disaggregation and the necessity of additional verifications of the
721 overlapping moving window algorithm for other gauges with longer and better quality
722 observational time series.

723 Returning to questions of interest in urban hydrology addressed at the end of
724 Introduction we can formulate following answers:

- 725 1) Small precipitation variability within gauges located in city centered, as measured
726 via microcanonical cascade generators, justifies the practice of a single time series
727 for the probabilistic assessment of the entire urban drainage system.
- 728 2) From current engineering needs in urban hydrology, it is enough to use only one
729 fitted MCM for the precipitation time series disaggregation in Warsaw city. We

730 suppose that this result could be valid even in larger urban areas, but the
731 verification is necessary. We dissuade from the cascade generation fitted on
732 precipitation time series collected at instruments located out of the city center in
733 unrepresentative sites, like in our case, the ground of the airport.

734 3) We question the practice of using gauges from airport for urban hydrology.
735 Finally, we recommend further research to assess the influence of the local conditions on
736 BDC histograms to find more clear explanations of observed anomalies. We also recognize
737 the necessity of further tests on other cities and precipitation monitoring networks, especially
738 in case of cities with complicated orography and presence of hydrological networks.

739

740 **Acknowledgements**

741 This project was financed by the Polish National Science Centre (NCN) funds allocated on
742 basis of decision no 2011/03/B/ST10/06338. It was realized as a part of scientific project:
743 “Spatio-temporal analysis and modeling of urban precipitation field.” Precipitation data was
744 provided by the Municipal Water Supply and Sewerage Company (MWSSC) in Warsaw,
745 Poland. Authors also acknowledge the three anonymous reviewers for their suggestions and
746 comments.

747

748

749

750

751
752
753
754
755
756
757
758
759
760
761
762
763
764
765
766
767
768
769
770
771
772
773
774

References

Ahrens, B.: Rainfall downscaling in an alpine watershed applying a multiresolution approach, *J. Geophys. Res.*, 108, 8388, doi:10.1029/2001JD001485, 2003.

Arbeitsblatt DWA-A 117.: Bemessung von Regenrückhalteräumen. Deutsche Vereinigung für Wasserwirtschaft, Abwasser und Abfall e. V., Hennef, 2006.

Appendix B. Report on Approaches to UWWTD Compliance in Relation to CSO's in major cities across the EU. Thames Tunnel Needs Report, 2010.

Berne, A., Delrieu, G., Creutin, J.D. and Obled, C.: Temporal and spatial resolution of rainfall measurements required for urban hydrology. *J. Hydrol.*, 299(3-4), 166-179, doi: 10.1016/j.jhydrol.2004.08.002, 2004.

Cârsteanu, A., and Foufoula-Georgiou, E.: Assessing dependence among weights in a multiplicative cascade model of temporal rainfall, *J. Geophys. Res.* 101, D21, 26363-26370, doi: 10.1029/96JD01657, 1996.

De Michele, C., Salvadori, G., Vezzoli, R. and Pecora, S.: Multivariate assessment of droughts: Frequency analysis and dynamic return period, *Water Resour. Res.*, 49, 6985–6994, doi:10.1002/wrcr.20551, 2013.

EN 752, Drain and sewer systems outside buildings, 1997.

775 Fortuniak, K., Klysik, K., and Wibig, J.: Urban–rural contrasts of meteorological parameters
776 in Lodz. *Theor. Appl. Climatol.*, 84, 91–101, doi: 10.1007/s00704-005-0147-y, 2006.
777

778 Gires, A., Onof C., Maksimovic C., Schertzer D., Tchiguirinskaia I., and Simoes N.:
779 Quantifying the impact of small scale unmeasured rainfall variability on urban hydrology
780 through multifractal downscaling: a case study. *J. Hydrol.*, 442–443, 117–128, doi:
781 10.1016/j.jhydrol.2012.04.005, 2012.
782

783 Gires, A., Tchiguirinskaia, I., Schertzer, D. and Lovejoy, S.: Multifractal analysis of an urban
784 hydrological model on a Seine-Saint-Denis study case. *Urban Water J.*, 10(3), 195-208, doi:
785 10.1080/1573062X.2012.716447, 2013.
786

787 Górski J.: Analysis of Precipitation Time Series for Needs of Urban Hydrology on Example
788 of Kielce City. PhD thesis (in Polish), Kielce University of Technology, 2013.
789

790 Harris, D., A. Seed, Menabde M., and Austin G.: Factors affecting multiscaling analysis of
791 rainfall time series, *Nonlin. Processes Geophys.* 4, 3, 137-156, doi: 10.5194/npg-4-137-1997,
792 1997.
793

794 Hingray B., and Ben Haha, M.: Statistical performances of various deterministic and
795 stochastic models for rainfall series disaggregation. *Atmos. Res.*, 77, 152– 175, 2005.
796

797 Kłysik, K., and Fortuniak, K.: Temporal and spatial characteristics of the urban heat island of
798 Łódź, Poland. *Atmos. Environ.*, **33**, 3885–3895, 1999.
799

800 Koutsoyiannis, D.: Rainfall disaggregation methods: Theory and applications, in: D. Piccolo
801 and L. Ubertini (eds.), Proc. Workshop on Statistical and Mathematical Methods for
802 Hydrological Analysis, Rome, 1-23, Università di Roma "La Sapienza",
803 <http://itia.ntua.gr/en/docinfo/570>, 2003.

804

805 Lanza L., Leroy M., Alexandropoulos C., Stagi L., and Wauben W.: WMO laboratory
806 intercomparison of rainfall intensity gauges. Final report. IOM Report No. 84, WMO/TD No.
807 1304, 2005.

808

809 Larose, D. T.: Discovering knowledge in data: an introduction to data mining. John Wiley &
810 Sons, Inc., Hoboken, New Jersey, 2005.

811

812 Licznar, P.: Stormwater reservoir dimensioning based on synthetic rainfall time series.
813 Ochrona Srodowiska, 35(2), 27–32, 2013.

814

815 Licznar, P., Łomotowski, J., and Rupp, D. E.: Random cascade driven rainfall disaggregation
816 for urban hydrology: An evaluation of six models and a new generator, Atmos. Res. 99, 3-4,
817 563-578, doi:10.1016/j.atmosres.2010.12.014, 2011a.

818

819 Licznar, P., Schmitt, T. G., and Rupp, D. E.: Distributions of microcanonical cascade weights
820 of rainfall at small timescales, Acta Geophysica, 59 (5), 1013-1043, doi:10.2478/s11600-011-
821 0014-4, 2011b.

822

823 Lombardo, F., Volpi, E., and Koutsoyiannis, D.: Rainfall downscaling in time: theoretical and
824 empirical comparison between multifractal and Hurst-Kolmogorov discrete random cascades,
825 *Hydrolog. Sci. J.*, 57(6), 1052-1066, doi: 10.1080/02626667.2012.695872, 2012.

826

827 Marshak, A., Davis, A., Cahalan, R., and Wiscombe, W.: Bounded cascade models as
828 nonstationary multifractals, *Phys. Rev. E*, 49,55-69, 1994.

829

830 Menabde, M., and Sivapalan, M.: Modeling of rainfall time series and extremes using
831 bounded random cascades and Levy-stable distributions, *Water Resour. Res.*, 36(11), 3293–
832 3300, doi:10.1029/2000WR900197, 2000.

833

834 Menabde, M., D. Harris, A. Seed, G. Austin, and Stow D.: Multiscaling properties of rainfall
835 and bounded random cascades, *Water Resour. Res.* 33, 12, 2823-2830, doi:
836 10.1029/97WR02006, 1997.

837

838 Molnar, P., and Burlando, P.: Preservation of rainfall properties in stochastic disaggregation
839 by a simple random cascade model, *Atmos. Res.*, 77, 1-4, 137-151,
840 doi:10.1016/j.atmosres.2004.10.024, 2005.

841

842 Molnar, P., and Burlando, P.: Variability in the scale properties of high-resolution
843 precipitation data in the Alpine climate of Switzerland, *Wat. Resour. Res.*, 44, W10404,
844 doi:10.1029/2007WR006142, 2008.

845

846 Oke T.: Initial guidance to obtain representative meteorological observations at urban sites,
847 Instruments and Observing Methods, Report no. 81, World Meteorological Organization,
848 WMO/TD-No. 1250, 2006.

849

850 Olsson J.: Evaluation of a scaling cascade model for temporal rainfall disaggregation, *Hydrol.*
851 *Earth Syst. Sci.*, 2, 19-30, DOI: 10.5194/hess-2-19-1998, 1998.

852

853 Over, T. M., and Gupta V. K.: A space-time theory of mesoscale rainfall using random
854 cascades. *J. Geophys. Res.*, 101(D21), 26319-26331. 1996

855

856 Paulson, K.S., and Baxter P. D.: Downscaling of rain gauge time series by multiplicative beta
857 cascade, *J. Geophys. Res.* 112, D09105, doi: 10.1029/2006JD007333, 2007.

858

859 Peng, S., Piao, S., Ciais, P., Friedlingstein P., Oettle C., Bréon F.-M. Nan H., Zhou L. and
860 Myneni R.B.: Surface Urban heat island across 419 global big cities, *Environ. Sci.*
861 *Technol.*, 2012, 46 (2), 696–703, doi: 10.1021/es2030438, 2012.

862

863

864 Robert, C.P.: Simulation of truncated normal variables, *Statistics and Computing* 5, 121–125,
865 1995.

866

867 Rupp, D. E., Keim, R. F., Ossiander, M., Brugnach, M., and Selker, J. S.: Time scale and
868 intensity dependency in multiplicative cascades for temporal rainfall disaggregation, *Water*
869 *Resour. Res.*, 45, W07409, doi:10.1029/2008WR007321, 2009.

870

871 Rupp D. E., P. Licznar, W. Adamowski, and Leśniewski M.: Multiplicative cascade models
872 for fine spatial downscaling of rainfall: parameterization with rain gauge data. *Hydrol. Earth*
873 *Syst. Sci.*, 16, 671–684, doi:10.5194/hess-16-671-2012, 2012.

874

875 Schmitt, T. G.: *ATV-DVWK Kommentar, ATV-A 118 Hydraulische Berechnung von*
876 *Entwässerungssystemen*, DWA, Hennef, 2000.

877

878 Willems, P.: Multidecadal oscillatory behaviour of rainfall extremes. *Clim. Chang.*, 120, 931–
879 944, doi: 10.1007/s10584-013-0837-x, 2013.

880

881 WMO-No. 8, *Guide to Meteorological Instruments and Methods of Observation*. World
882 *Meteorological Organization - WMO*, 2012.

883

884

885
886
887

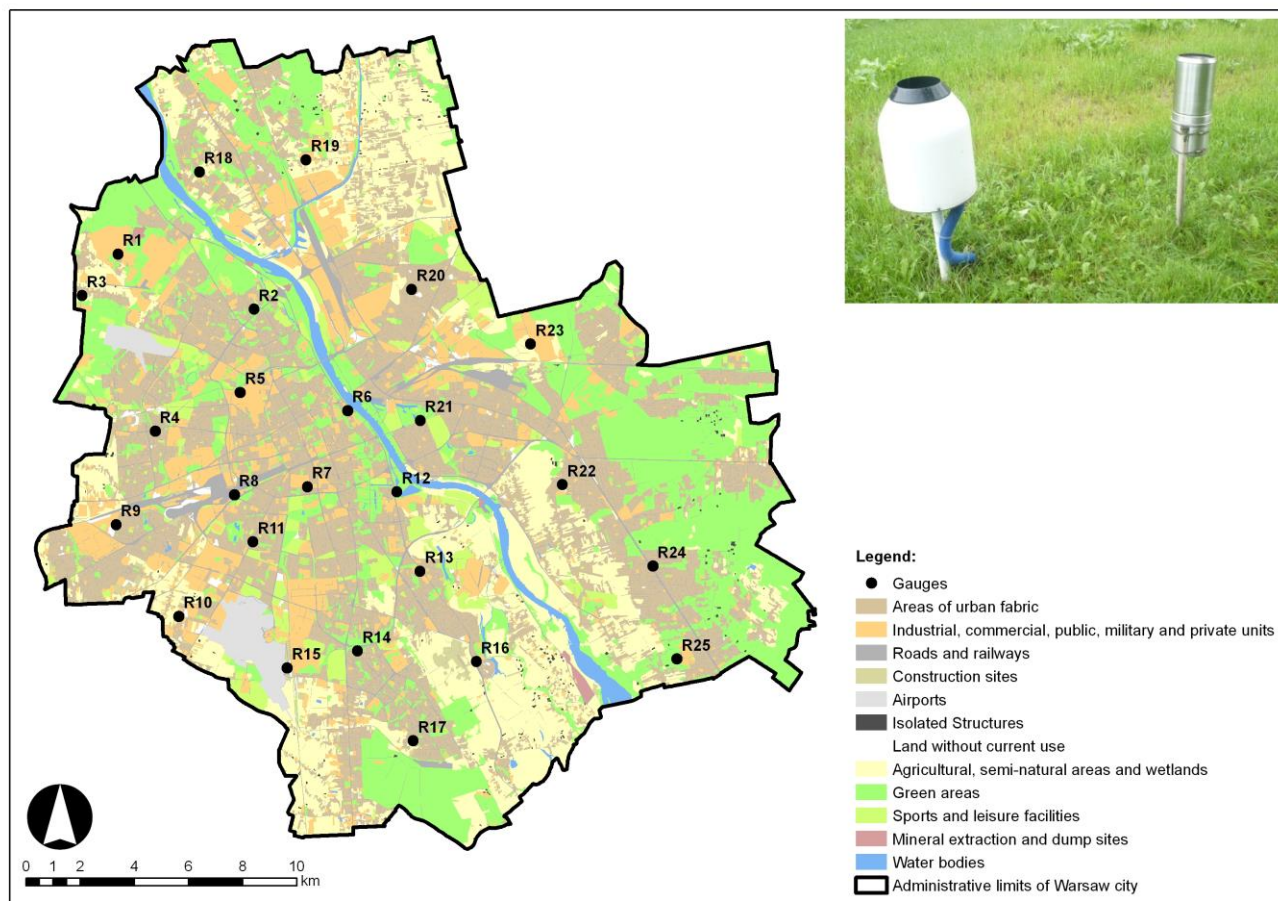
Tab. 1. Values of p_1 , p_2 , a , σ_1 and σ_2 parameters at different timescales, for gauge R7. The values of parameters are reported in bold, whereas their 95% confidence limits are in italic.

Breakdown times	Timescale	p_1	p_2	a	σ_1	σ_2
5-10 min.	$\lambda=1$	0.1541	0.3479	1.3350	0.0559	0.1341
		<i>0.1474</i>	<i>0.3377</i>	<i>1.3097</i>	<i>0.0523</i>	<i>0.1300</i>
		<i>0.1608</i>	<i>0.3580</i>	<i>1.3604</i>	<i>0.0595</i>	<i>0.1383</i>
10-20 min.	$\lambda=2$	0.0706	0.4036	1.0632	0.0559	0.1341
		<i>0.0644</i>	<i>0.3950</i>	<i>1.0474</i>	<i>0.0523</i>	<i>0.1300</i>
		<i>0.0768</i>	<i>0.4121</i>	<i>1.0789</i>	<i>0.0595</i>	<i>0.1383</i>
20-40 min.	$\lambda=4$	0.0212	0.5036	0.9437	0.0559	0.1341
		<i>0.0155</i>	<i>0.4954</i>	<i>0.9325</i>	<i>0.0523</i>	<i>0.1300</i>
		<i>0.0270</i>	<i>0.5118</i>	<i>0.9548</i>	<i>0.0595</i>	<i>0.1383</i>
40-80 min.	$\lambda=8$	-	0.6175	0.9484	-	0.1341
		-	<i>0.6091</i>	<i>0.9390</i>	-	<i>0.1300</i>
		-	<i>0.6259</i>	<i>0.9579</i>	-	<i>0.1383</i>
80-160 min.	$\lambda=16$	-	0.7548	0.9170	-	0.1341
		-	<i>0.7494</i>	<i>0.9098</i>	-	<i>0.1300</i>
		-	<i>0.7601</i>	<i>0.9242</i>	-	<i>0.1383</i>
160-320 min.	$\lambda=32$	-	0.8873	0.8929	-	0.1341
		-	<i>0.8827</i>	<i>0.8873</i>	-	<i>0.1300</i>
		-	<i>0.8919</i>	<i>0.8985</i>	-	<i>0.1383</i>
320-640 min.	$\lambda=64$	-	0.9797	0.8799	-	0.1341
		-	<i>0.9758</i>	<i>0.8754</i>	-	<i>0.1300</i>
		-	<i>0.9835</i>	<i>0.8843</i>	-	<i>0.1383</i>
640-1280 min.	$\lambda=128$	-	1.0000	0.7783	-	0.1341
		-	<i>0.9973</i>	<i>0.7754</i>	-	<i>0.1300</i>
		-	<i>1.0027</i>	<i>0.7813</i>	-	<i>0.1383</i>

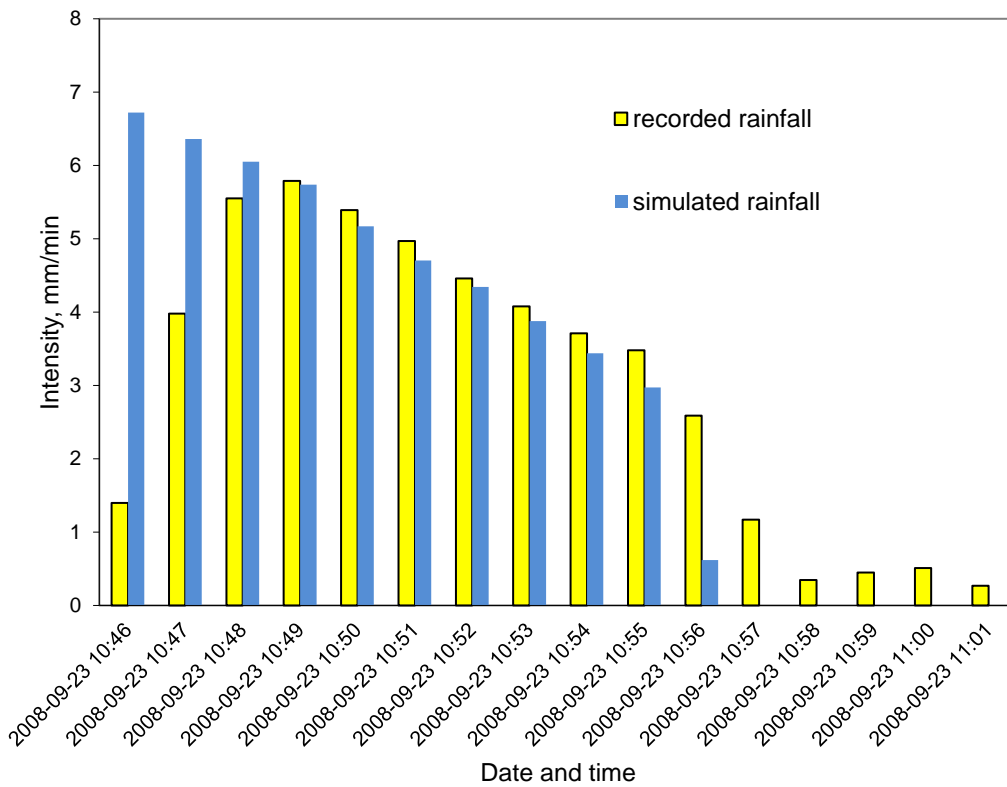
888

889 Tab. 2. Values of the Akaike information criterion (AIC) for 2N-B distribution (model 1) -- or its simplifications
 890 N-B and B -- and Beta B distribution (model 2), and the hierarchy of analyzed timescales λ , at gauge R7.
 891 Calculations were based on estimates of the maximized value of the log-likelihood function (LL) known sample
 892 size (n) and number of model parameters (k).
 893

Breakdown times	Timescale	n	Model 1				Model 2				$\Delta = \text{AIC(M2)} - \text{AIC(M1)}$
			Distr.	k	LL	AIC(M1)	Distr.	k	LL	AIC(M2)	
5-10 min.	$\lambda=1$	132940	2N-B	5	48480	-96950	B	1	36307	-72612	24338
10-20 min.	$\lambda=2$	136968	2N-B	5	32272	-64534	B	1	19798	-39593	24941
20-40 min.	$\lambda=4$	144778	2N-B	5	19071	-38132	B	1	8794	-17585	20547
40-80 min.	$\lambda=8$	159272	N-B	3	11119	-22232	B	1	4464	-8927	13305
80-160 min.	$\lambda=16$	185014	N-B	3	4591.9	-9178	B	1	925	-1848	7330
160-320 min.	$\lambda=32$	230716	N-B	3	1167.3	-2329	B	1	46	-91	2238
320-640 min.	$\lambda=64$	315360	N-B	3	1543.70	-3081	B	1	1491	-2979	102
640-1280 min.	$\lambda=128$	501092	B	1	12614.40	-25227	B	1	12614	-25227	0



894
 895 Fig. 1. Map of 25 gauges composing the precipitation-monitoring network in Warsaw. Administrative limits of Warsaw city and limits of forested areas were marked in
 896 black. The land use classification of was made through the Urban Atlas, which provides pan-European comparable land use and land cover data for large urban zones with
 897 more than 100.000 inhabitants (<http://www.eea.europa.eu/data-and-maps/data/urban-atlas#tab-metadata>). The average density of network is 1 instrument over 20.7 km². MPS
 898 weighing-type TRwS 200E gauges were accompanied with standard Hellman gauges for the routine control of daily precipitation totals.



900
901
902
903

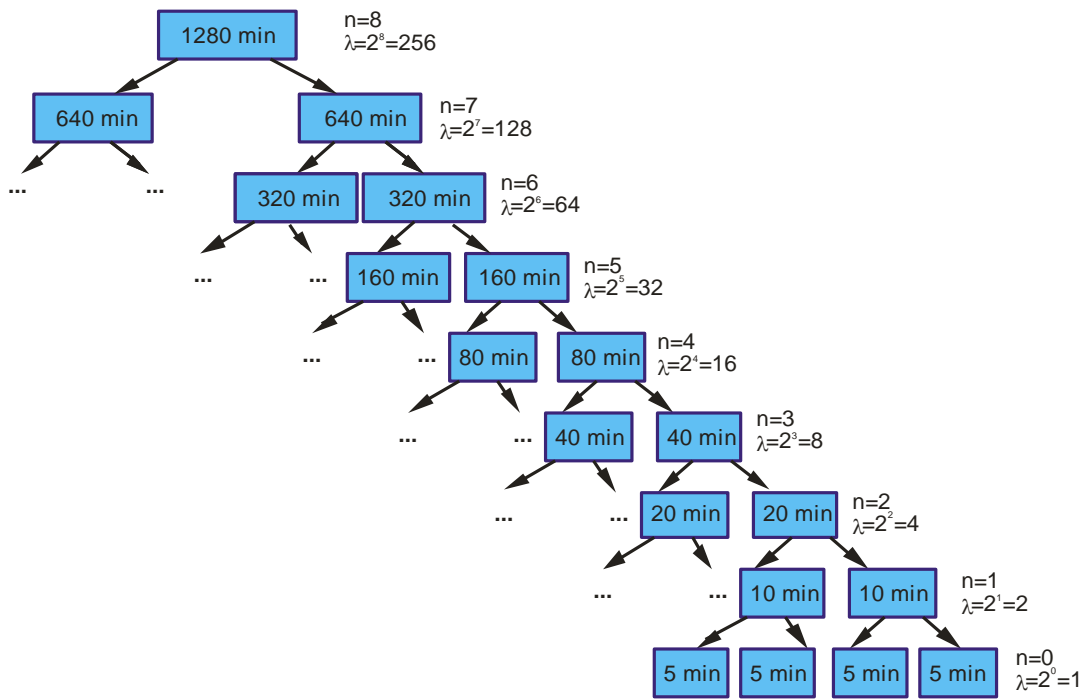
Fig. 2. Weighing-type TRwS 200E gauge during some tests (upper panel). Rainfall is simulated by means of precise medical pump. Sample of test results reporting simulated and recorded rainfall depths (lower panel).



904
905

906
907
908
909

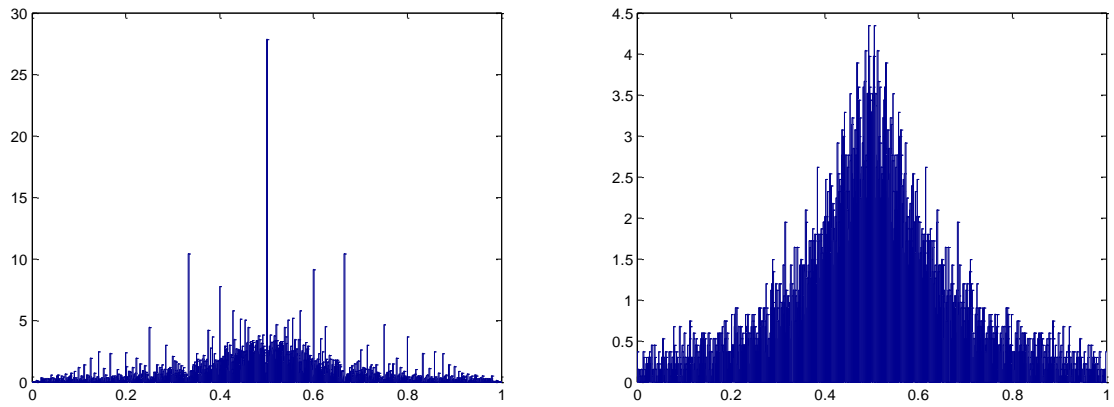
Fig. 3. Location of Polish and German precipitation gauges used during the comparison of Warsaw results with other studies.



910
 911
 912
 913
 914
 915

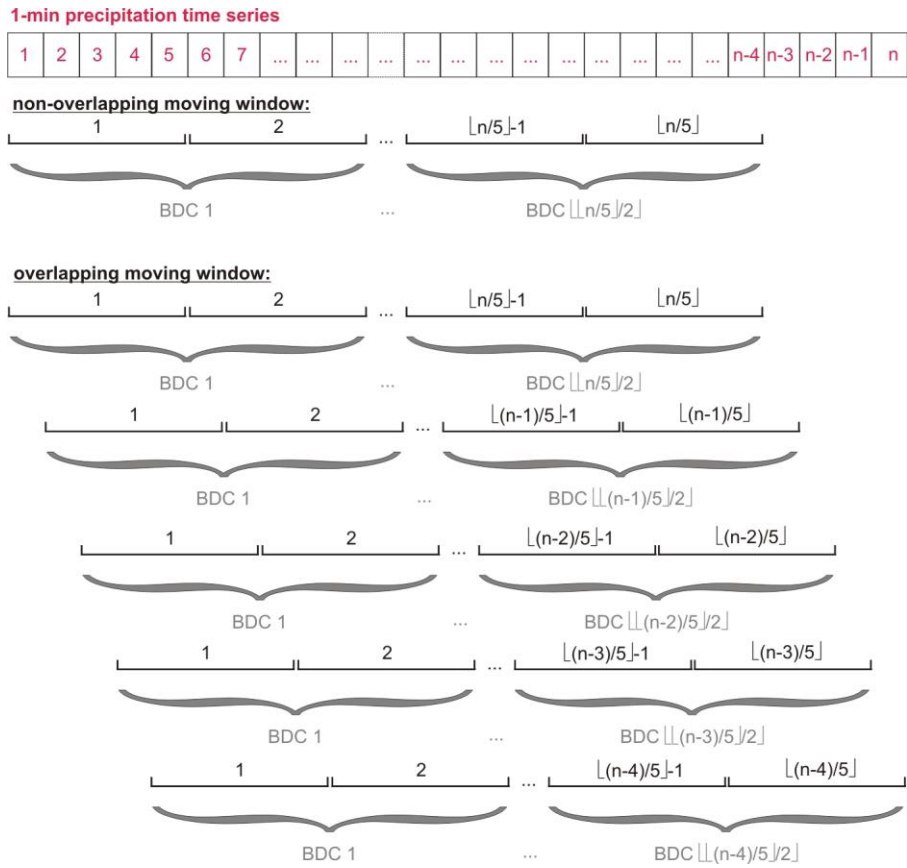
Fig. 4. Schematic diagram of developed microcanonical cascade model with branching number $b=2$.

916
917



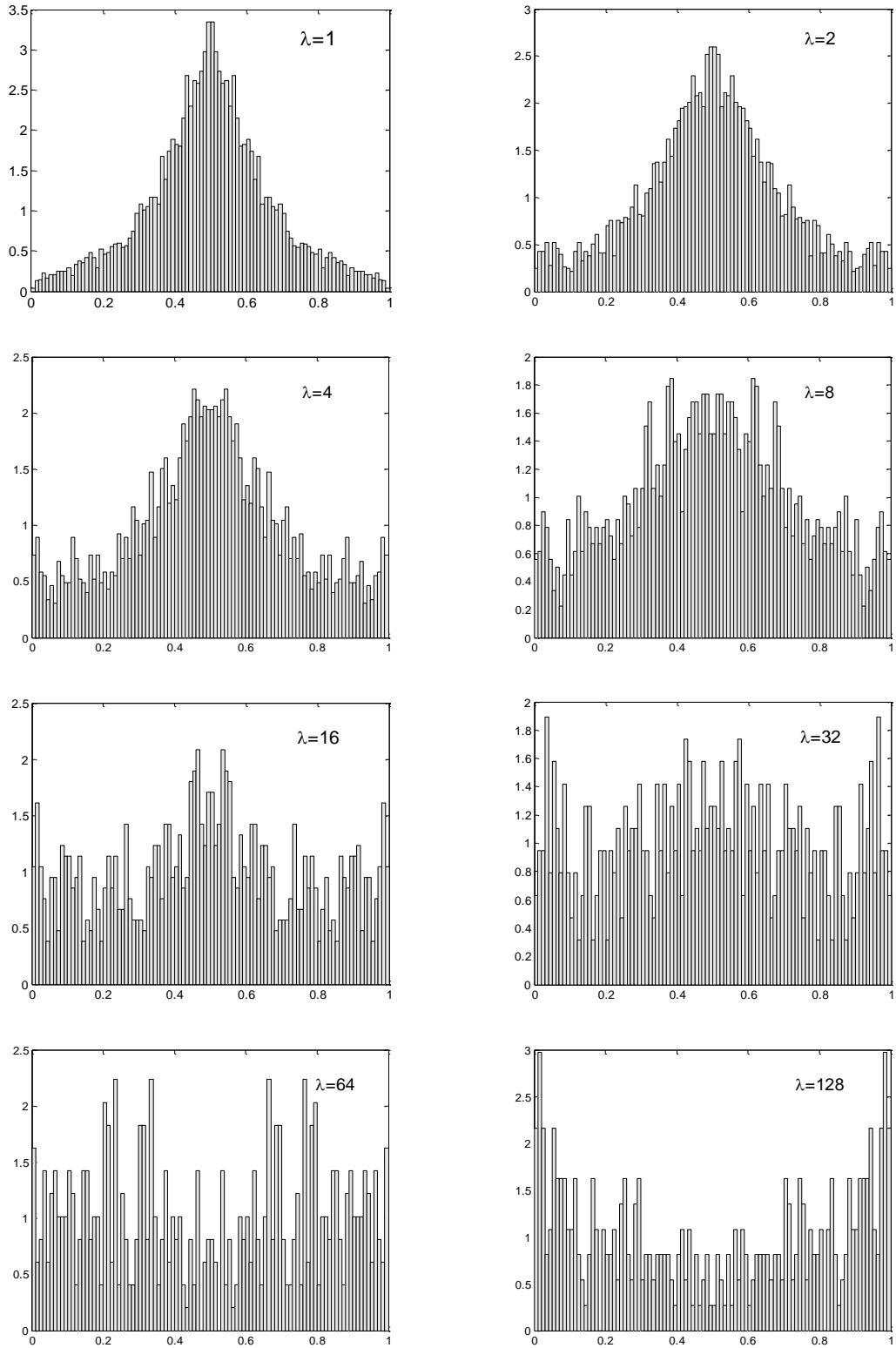
918
919
920
921
922

Fig. 5. Comparison of BDC histograms for gauge R7, and timescale $\lambda=1$, calculated according to the non-overlapping moving window algorithm and using original (left panel), and randomized (right panel) non-zero precipitation data. Horizontal axes show BDC range, and vertical axes the respective frequency values.



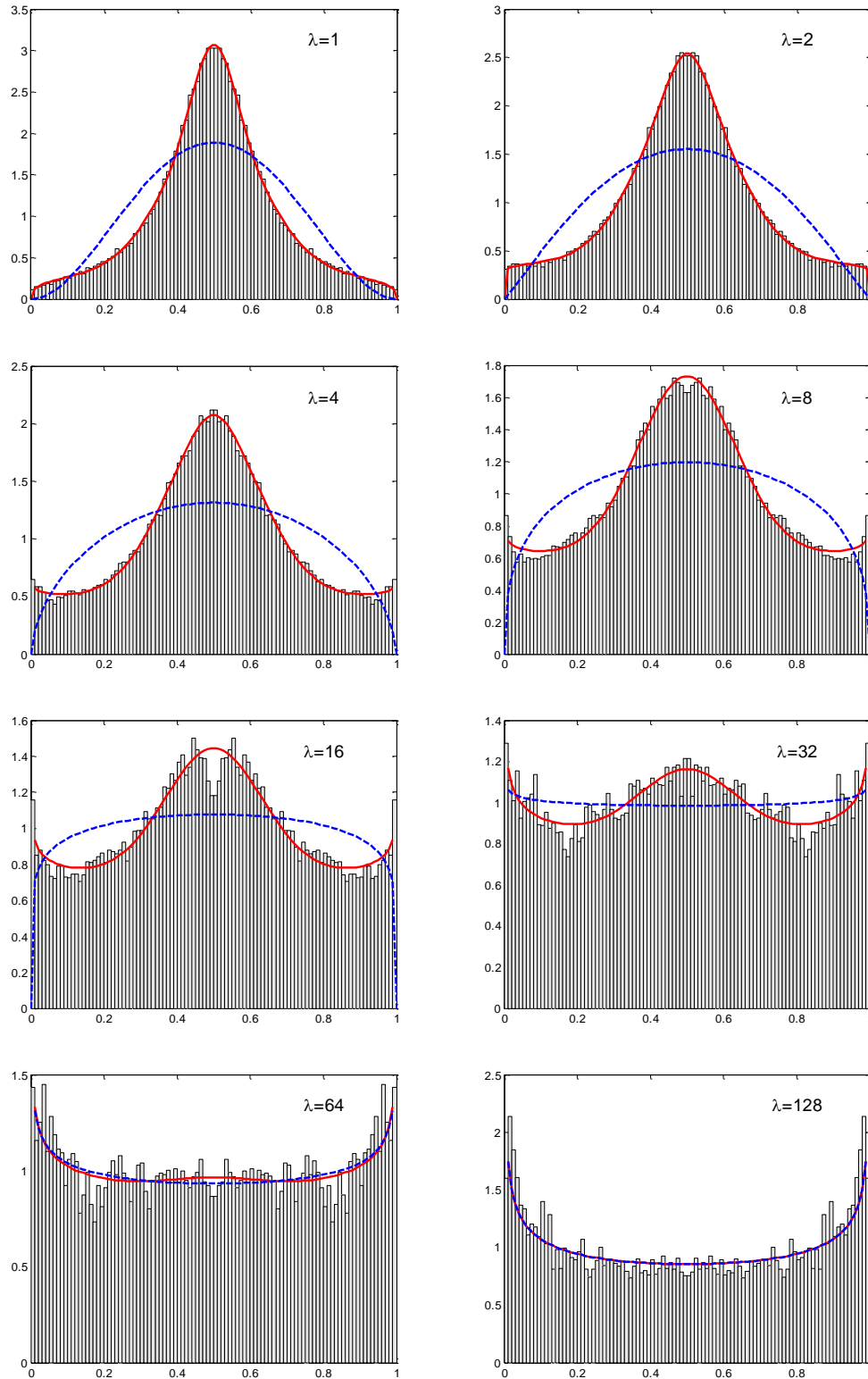
923
924
925
926
927
928

Fig. 6. Example showing differences between non-overlapping and overlapping moving window algorithms for the calculation of BDCs in case of 1-min precipitation time series and breakdown time 5-10 min. Note that $\lfloor n \rfloor$ means the integer part of n , where n is the total length of 1-min precipitation time series.



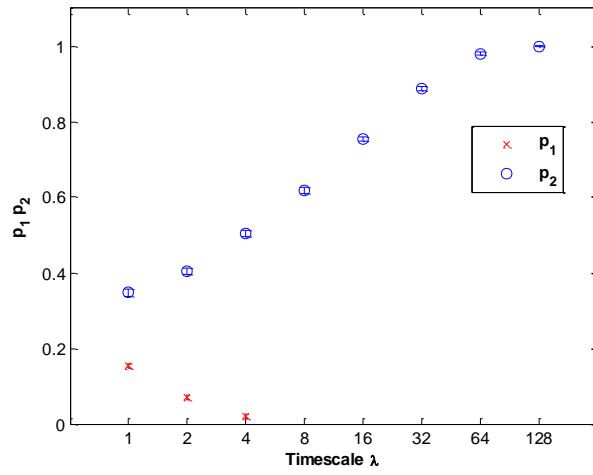
929
 930
 931
 932
 933

Fig. 7. Histograms of BDC values for gauge R7 calculated according to the non-overlapping moving window algorithm and based on randomized precipitation time series. Horizontal axes show BDC range and vertical axes the respective frequency values.



934 Fig. 8. Histograms of BDC values calculated according to overlapping moving window algorithm and based on
 935 randomized gauge R7 precipitation times series. Horizontal axes show BDC range and vertical axes the
 936 respective frequency values. The solid red curves represent the 2N-B probability density function, whereas the
 937 blue dashed curves the Beta probability density function.
 938

939



940
941
942
943

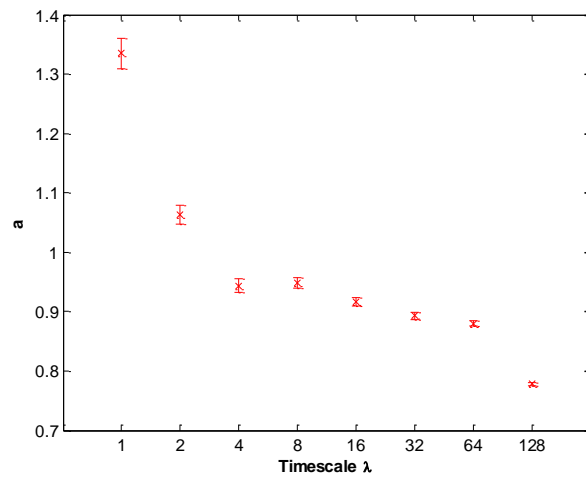
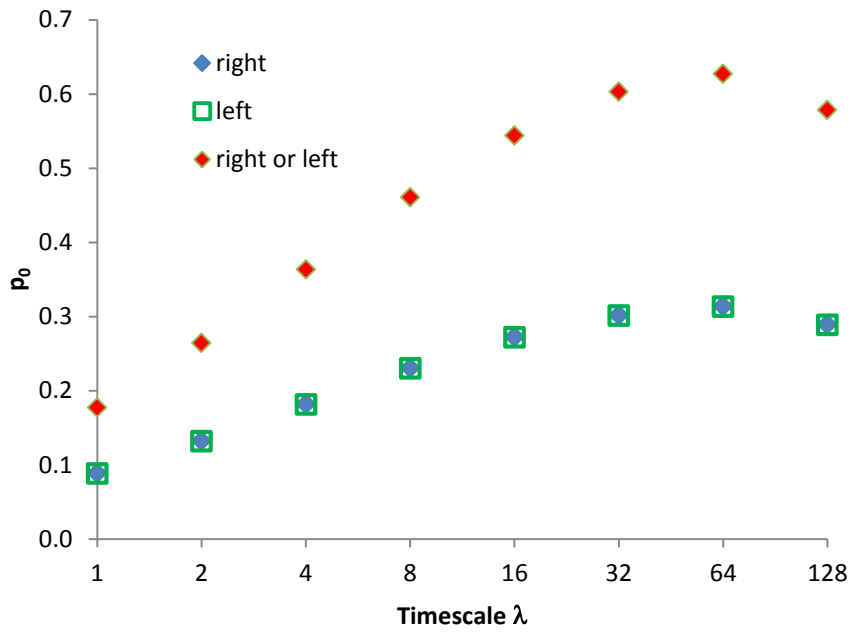
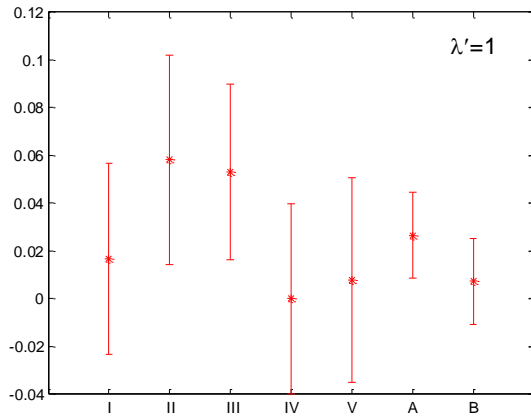


Fig. 9. Value and 95% confidence intervals of parameters of p_1, p_2 and a with λ , for gauge R7. Horizontal axes are plotted at binary logarithm scale \log_2 .



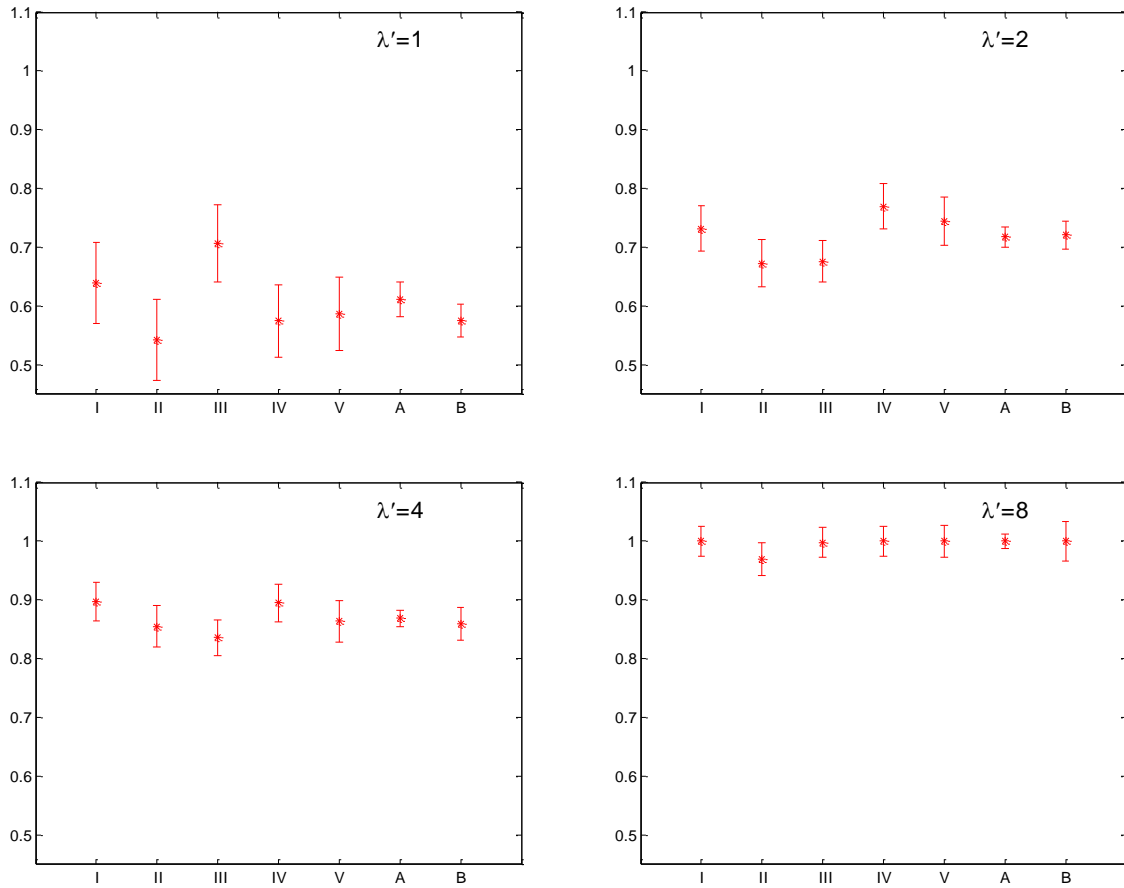
944
 945
 946
 947

Fig. 10. Variability of the intermittency parameter p_0 with λ , for gauge R7. Horizontal axis is plotted at binary logarithm scale \log_2 .

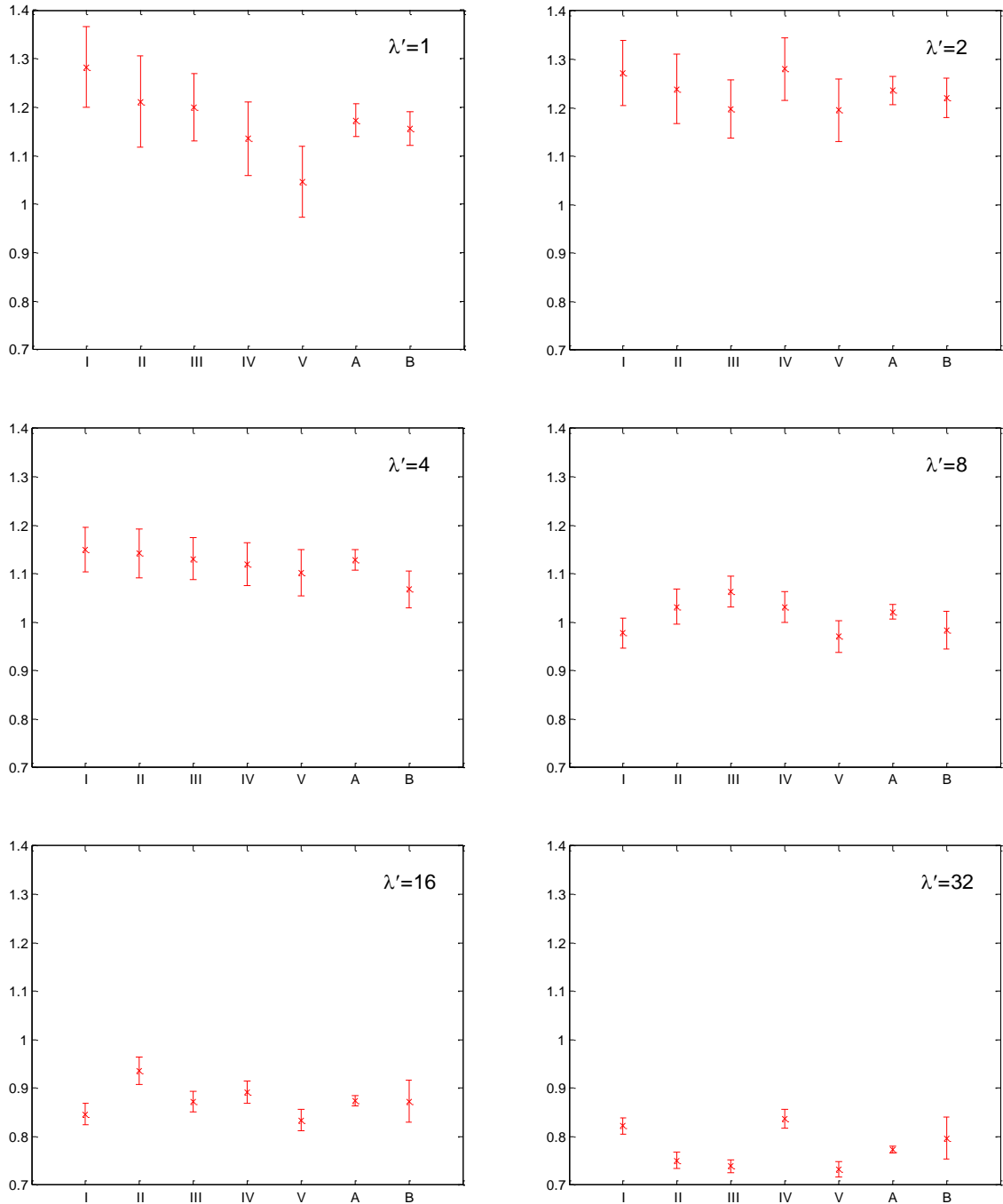


948

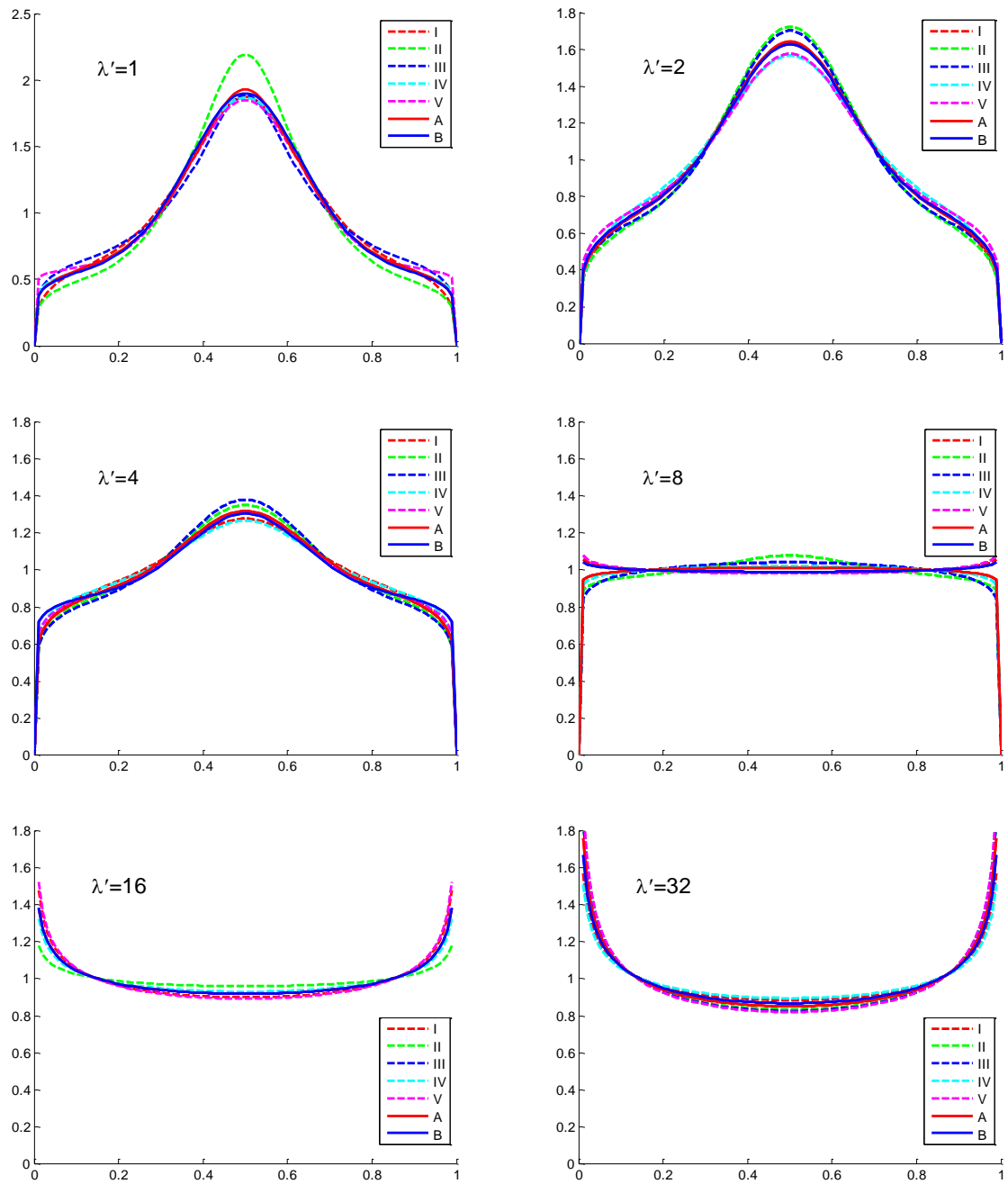
949 Fig. 11. Value and 95% confidence intervals of parameter p_1 at timescale $\lambda'=1$, for gauge R7. Roman numbers
 950 I-V on horizontal axes indicate respectively the 5-year ranges: 1983-1987, 1988-1992, 1993-1997, 1998-2002
 951 and 2003-2007. Uppercase letters A and B indicate values calculated using all 25-year range 1983-2007, and
 952 non-overlapping (A), overlapping (B) moving window algorithm.
 953



954 Fig. 12. Value and 95% confidence intervals of parameter p_2 at timescales $\lambda'=1,2,4,8$, for gauge R7.
 955 Roman numbers I-V on horizontal axes indicate respectively the 5-year ranges: 1983-1987, 1988-1992, 1993-1997,
 956 1998-2002 and 2003-2007. Uppercase letters A and B indicate values calculated using all 25-year range 1983-
 957 2007, and non-overlapping (A), overlapping (B) moving window algorithm.
 958

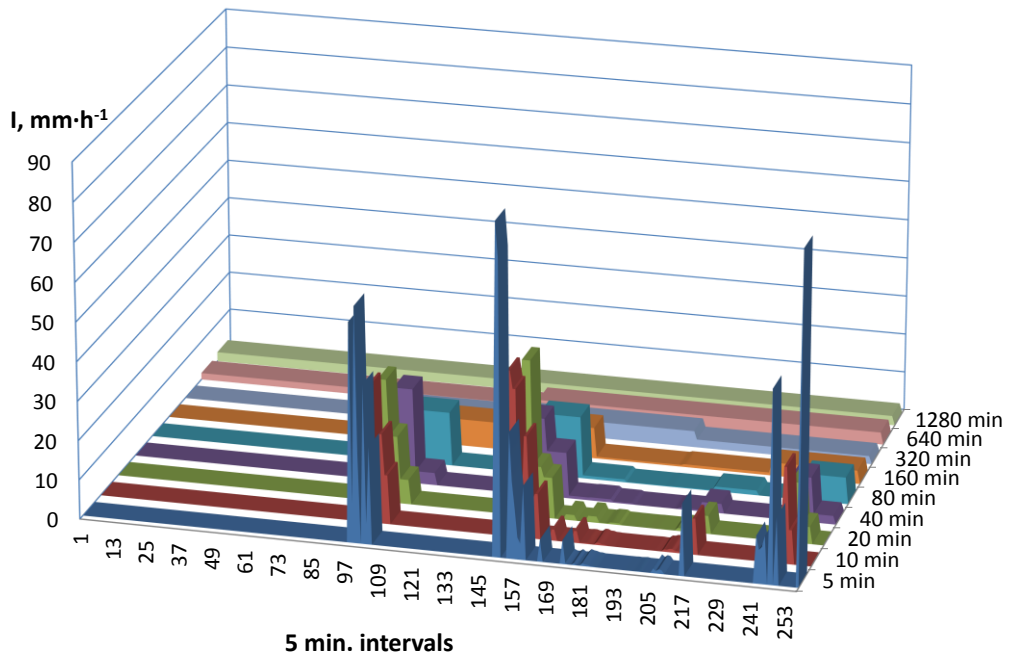


959 Fig. 13. Value and 95% confidence intervals of parameter a at timescales $\lambda'=1,2,4,8,16,32$, for gauge R7.
 960 Roman numbers I-IV on horizontal axes indicate respectively the 5-year ranges: 1983-1987, 1988-1992, 1993-
 961 1997, 1998-2002 and 2003-2007. Uppercase letters A and B indicate values calculated using all 25-year range
 962 1983-2007, and non-overlapping (A), overlapping (B) moving window algorithm.
 963
 964



965 Fig. 14. Variability of fitted theoretical BDCs distributions histograms at timescales $\lambda'=1,2,4,8,16,32$, for gauge
 966 R7. Roman numbers I-V in legend indicate respectively the 5-year ranges: 1983-1987, 1988-1992, 1993-1997,
 967 1998-2002 and 2003-2007. Uppercase letters A and B indicate results calculated using all 25-year range 1983-
 968 2007, and non-overlapping (A), overlapping (B) moving window algorithm. In all plots, horizontal axes show
 969 BDC ranges and vertical axes the frequency values.
 970

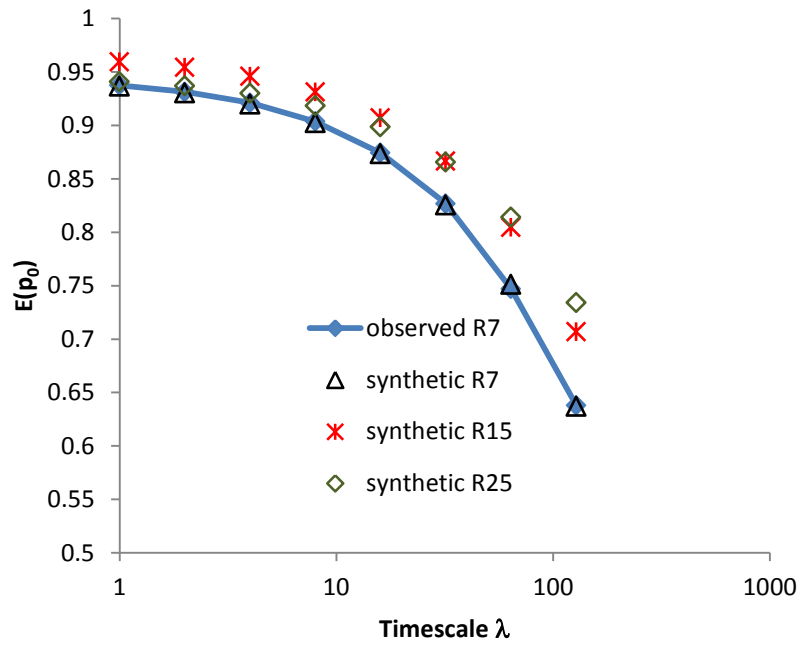
971
 972



973
974

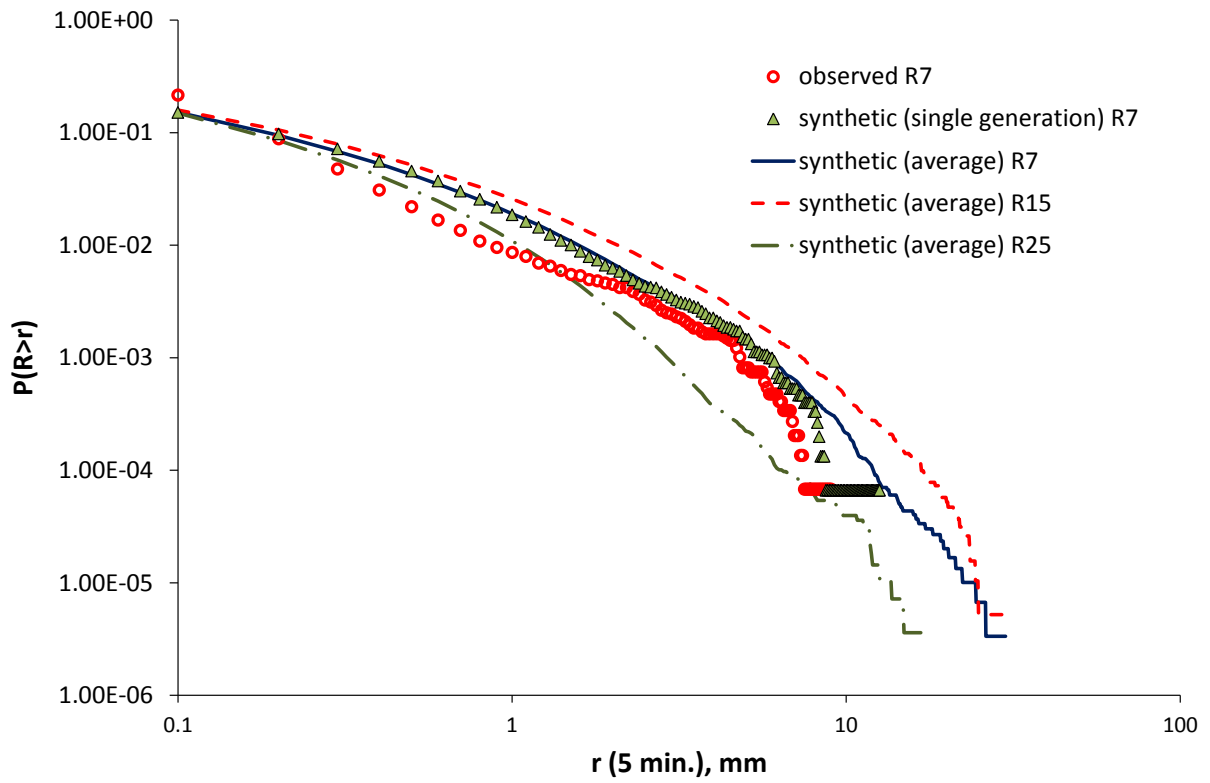
Fig. 15. An example of precipitation disaggregation of a 56.3 mm event from 1280 min to 5 min, for gauge R7.

975
976



977
978
979
980
981

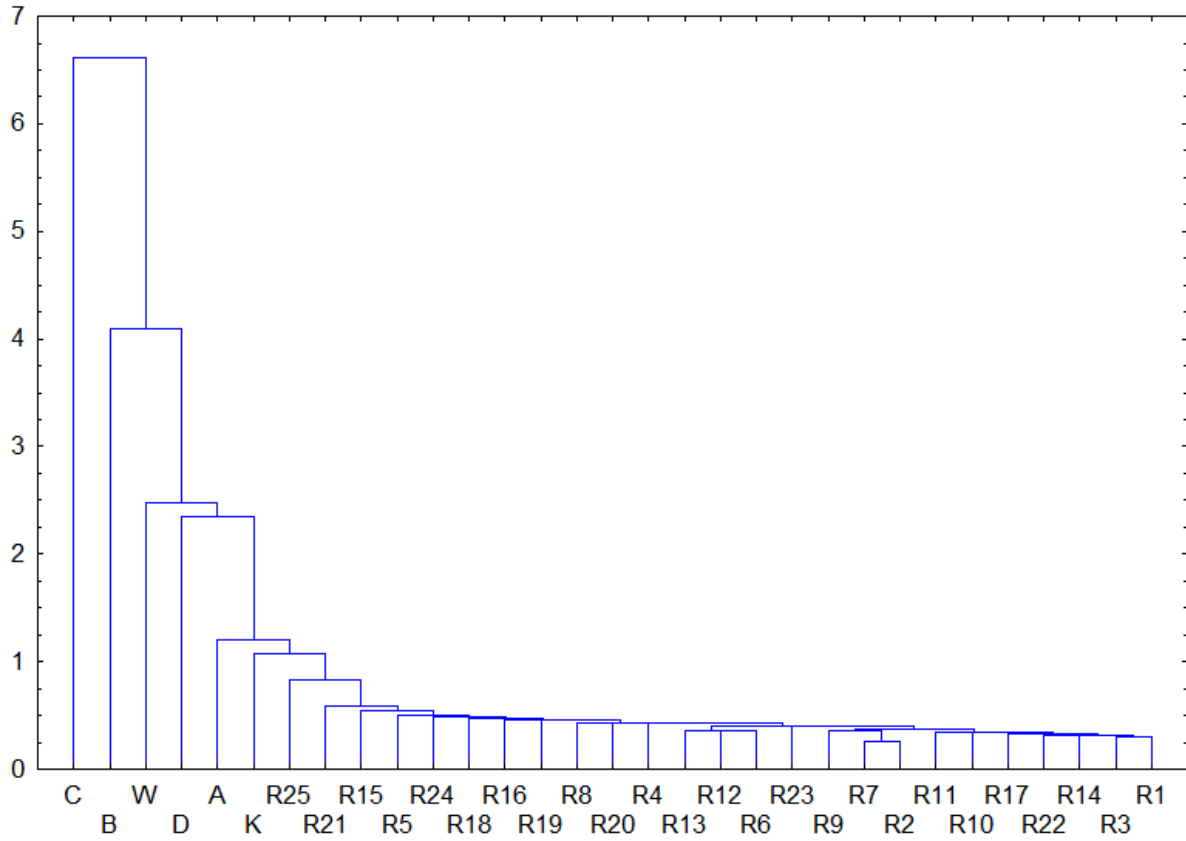
Fig. 16. Comparison between observed for gauge R7 and synthetic series for gauges R7, R15 and R25 in terms of intermittency $E(p_0)$ for the considered timescales. The values for the generated data are calculated as average of 100 disaggregation runs. The variability between runs was negligible and so is not shown here.



982
 983
 984
 985
 986
 987
 988
 989
 990

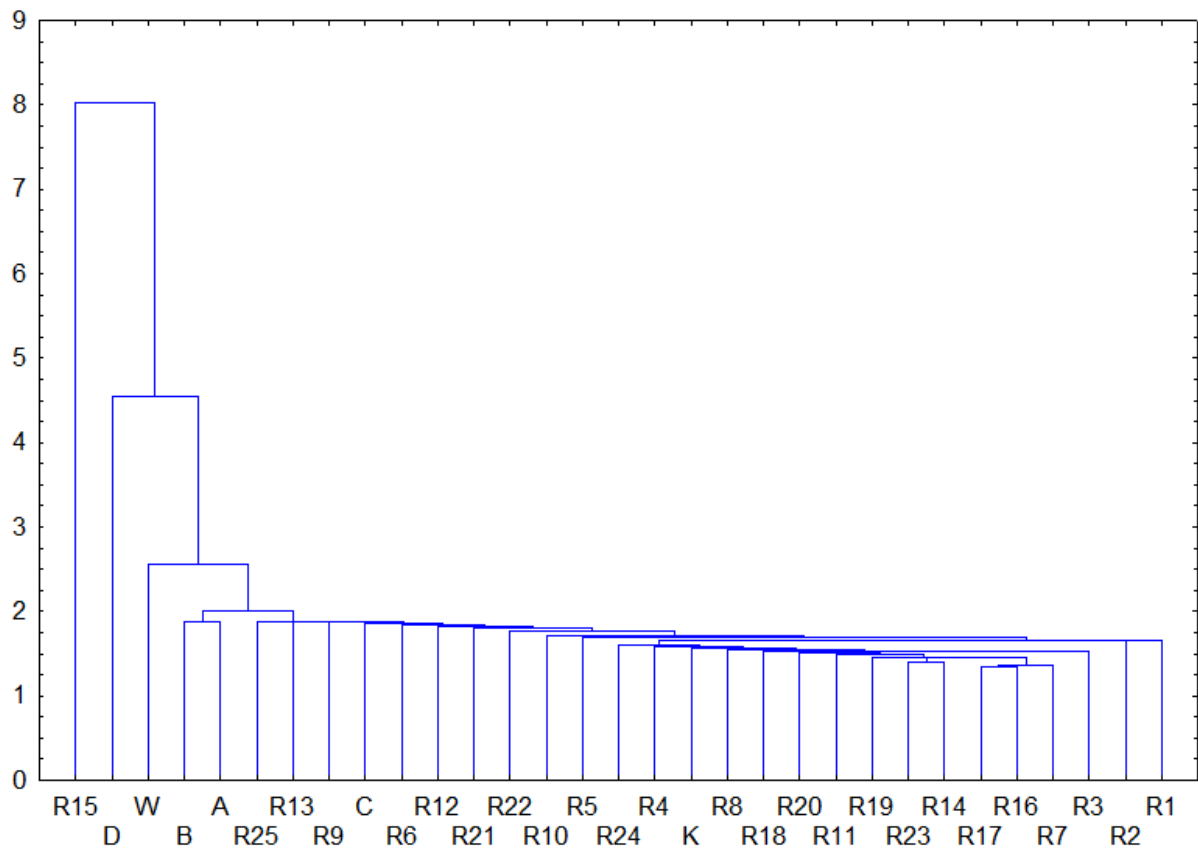
Fig. 17. The survival probability function of 5 min precipitation amounts for the observed time series (circles) and the synthetic time series (triangles) generated by the disaggregation of 1280 precipitation amounts, for gauge R7. The lines represent the average distributions calculated over the generation of 100 synthetic time series for gauge R7 and for comparison for gauges R15 and R25.

991



992
993
994
995
996
997

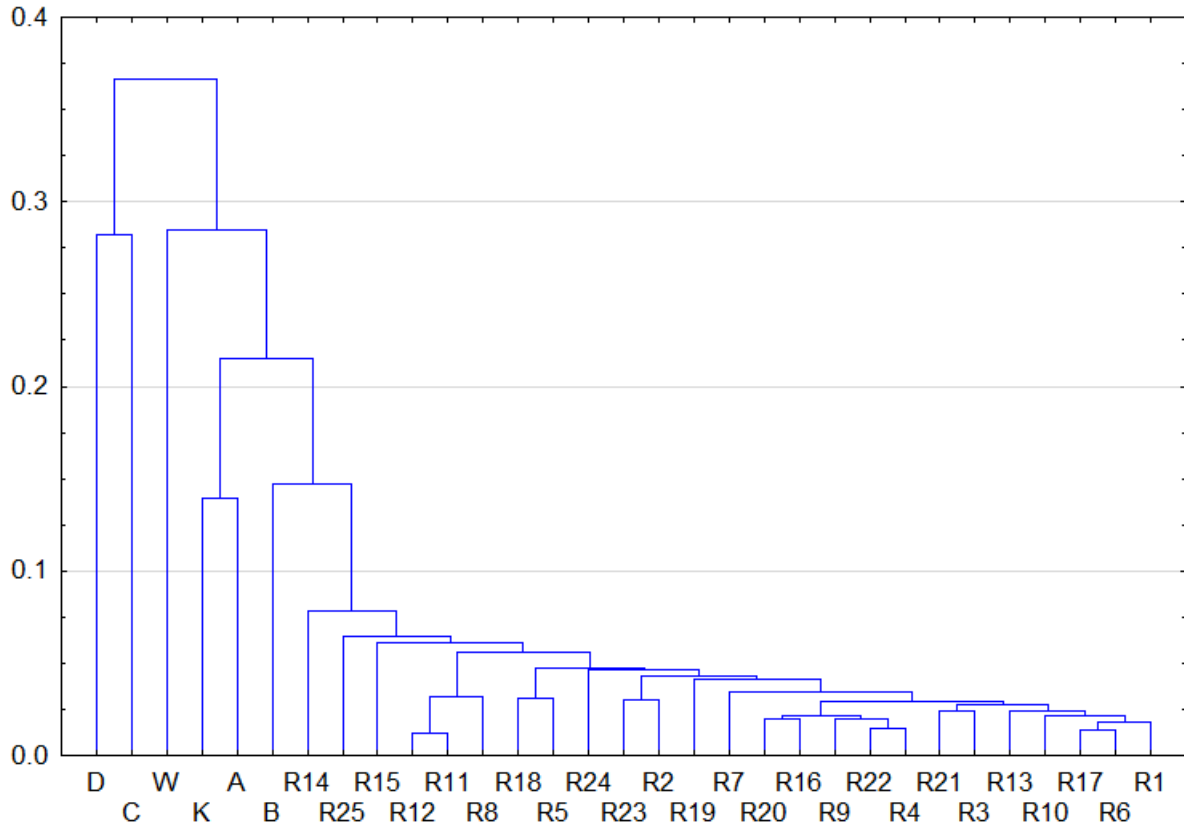
Fig. 18. Dendrogram resulting from the cluster analysis of BDC histograms for $\lambda=1$. The vertical scale shows binding distance, whereas names of gauges are given on horizontal scale (K stands for Kielce gauge, and W stands for Wroclaw).



998
 999
 1000
 1001
 1002
 1003

Fig. 19. Dendrogram resulting from the cluster analysis of BDCs histograms for the timescale $\lambda=128$. The vertical scale shows binding distance, whereas names of gauges are given on horizontal scale (K stands for Kielce gauge, and W stands for Wroclaw).

1004



1005
1006
1007
1008

Fig. 20. Dendrogram resulting from the cluster analysis of the intermittency parameter p_0 . The vertical scale shows binding distance, whereas the name of gauges is given on horizontal scale (K stands for Kielce gauge, and W stands for Wroclaw).